

Recent Developments in High-Temperature Permanent Magnet Materials

Contents

List of symbols

1. Introduction

1.1 Requirement for high-temperature permanent magnet materials

1.2 Review of conventional permanent magnet materials

2. Candidate alloy system for high-temperature permanent magnet materials

3. New Sm₂Co₁₇-based high-temperature permanent magnet materials

3.1 Effects of compositions on high-temperature intrinsic coercivity of Sm-TM permanent magnets

3.1.1 Effect of Sm on high-temperature intrinsic coercivity of Sm-TM permanent magnets

3.1.2 Effect of Fe on High Temperature mH_c of Sm-TM magnets

3.1.3. Effect of Cu on High Temperature mH_c of Sm-TM magnets

3.1.4. Effect of Zr on High Temperature mH_c of Sm-TM magnets

3.2. Magnetic properties of new Sm₂Co₁₇-based high-temperature permanent magnet materials

3.3 Dynamic characterizations of new high-temperature permanent magnets

3.4 Long-term thermal stability of new high-temperature permanent magnets

3.5 Microstructure and crystal structure

3.6 Coercivity in Sm-TM permanent magnets

3.6.1 Explanation of effects of Sm, Fe, Cu on intrinsic coercivity

3.6.2 Novel temperature dependence of intrinsic coercivity

4. New approach to calculating temperature coefficients of magnetic properties

5. SmCo₇-type permanent magnets

6. Temperature compensated rare earth permanent magnets and modeling of temperature coefficient of magnetization

7. Other high-temperature permanent magnet materials and future perspective

References

List of Symbols and Acronyms

| | |
|----------------------------------|--|
| $4\pi M$ | Magnetization |
| $4\pi M_s$ | Saturation magnetization |
| α_T | Temperature coefficient at T |
| $\alpha_{(T_1 \rightarrow T_2)}$ | Average temperature coefficient at $T_1 \rightarrow T_2$ |
| A | Exchange constant |
| β | Temperature coefficient of coercivity |
| B | Magnetic induction |
| $(BH)_{max}$ | Maximum energy product |
| B_r | Remanence |
| H | External applied field |
| H_A | Magneto-crystalline anisotropy field |
| H_k | Knee field |
| $M H_c$ | Intrinsic coercivity |
| HRE | Heavy rare earth |
| κ | Susceptibility |
| K | Crystalline anisotropy constant |
| k_B | Boltzmann constant |
| kG | Kilogauss |
| kOe | Kilo-Oersted |
| LRE | Light rare earth |
| μ | Permeability |
| MGOe | Megagauss Oersted |
| MM | Misch metal |
| ρ | Probability |
| RE | Rare earth |
| SEM | Scanning electron microscopy |
| SSHT | Solid solution heat treatment |
| T | Temperature |
| T_C | Curie temperature |
| TEM | Transmission electron microscopy |
| TM | Transition metal |
| T_M | Maximum temperature at which induction demagnetization curve remains a straight line |
| T_p | Temperature for peak magnetization |
| T_{rm} | Room temperature |
| XRD | X-ray diffraction |

List of Key Words

Aging, coercivity, coercivity mechanism, dynamic characterization, heavy rare earth, high temperature, abnormal temperature dependence of coercivity, permanent magnet, rare earth magnet, SmCo₅, SmCo₇, Sm₂Co₁₇, temperature coefficient, temperature compensation, temperature dependence, thermal activation, thermal stability

1. Introduction

1.1 Requirement for high-temperature permanent magnet materials

Permanent magnet materials capable of reliably operating at high temperatures ($\geq 400^\circ\text{C}$) are required for future advanced power systems in a proposed More Electric Aircraft (MEA) initiative. A major objective of the MEA initiative is to increase aircraft reliability, maintainability, and supportability, including drastically reducing the need for ground support equipment (Fingers et al. 2000). This advancement will be accomplished in part through the development of advanced power components such as magnetic bearings, integrated power units, and internal starter/generators for main propulsion engines. New high temperature magnets are enabling technologies for the development of these new power components. Power system designers frequently find that magnetic materials impose technological limitations on their designs. Compromises are generally required between the desired performance and the magnetic, mechanical, and electrical properties of available materials. If new materials can operate at $\geq 400^\circ\text{C}$, then new advanced designs will be possible. Air cooling, rather than complicated liquid cooling and its necessary logistics support, will become an operational capability. Likewise, oil-less/lubeless gas turbine engines and space power systems will be possible.

1.2 Review of conventional permanent magnet materials

Currently, the most widely-used permanent magnet materials are Alnico, hard ferrites, and high-performance rare earth-transition metal (RE-TM) permanent magnets, including SmCo_5 , $\text{Sm}_2(\text{Ce,Fe,Cu,Zr})_{17}$ ($\text{Sm}_2\text{TM}_{17}$ or 2:17), and Nd-Fe-B magnets. Table 1-1 lists the magnetic properties of some commercial magnets at room temperature. Figures 1-1 and 1-2 summarize the temperature dependence of the maximum energy product, $(\text{BH})_{\text{max}}$, and intrinsic coercivity, $M\text{H}_c$, for five types of commercial permanent magnetic materials (Walmer et al. 2000a). As shown in these figures, the magnetic properties of rare earth magnets are superior to all other magnet materials. Among rare earth magnets, Nd-Fe-B-type magnets have the highest static $(\text{BH})_{\text{max}}$ at temperatures $T < 130^\circ\text{C}$. At $T > 130^\circ\text{C}$, $\text{Sm}_2\text{TM}_{17}$ (2:17) magnets have the highest static $(\text{BH})_{\text{max}}$. The only magnet that maintains relatively high intrinsic coercivity (~ 10 kOe) at temperatures up to 300°C is $\text{Sm}_2\text{TM}_{17}$.

Table 1-1. Magnetic properties of some commercial permanent magnets at room temperature.

| Magnet | B_r (kG) | $M\text{H}_c$ (kOe) | $(\text{BH})_{\text{max}}$ (MGOe) | T_C ($^\circ\text{C}$) |
|-------------------------------------|---------------|------------------------|--------------------------------------|-------------------------------|
| Alnico 5 | 12 | 0.5 | 5 | 840 |
| Hard ferrite | 3.5 | 2.5 | 3 | 450 |
| SmCo_5 | 9 | 30 | 20 | 727 |
| $\text{Sm}_2\text{TM}_{17}$ | 11 | 30 | 28 | 820 |
| $\text{Nd}_2\text{Fe}_{14}\text{B}$ | 14 | 15 | 40 | 312 |

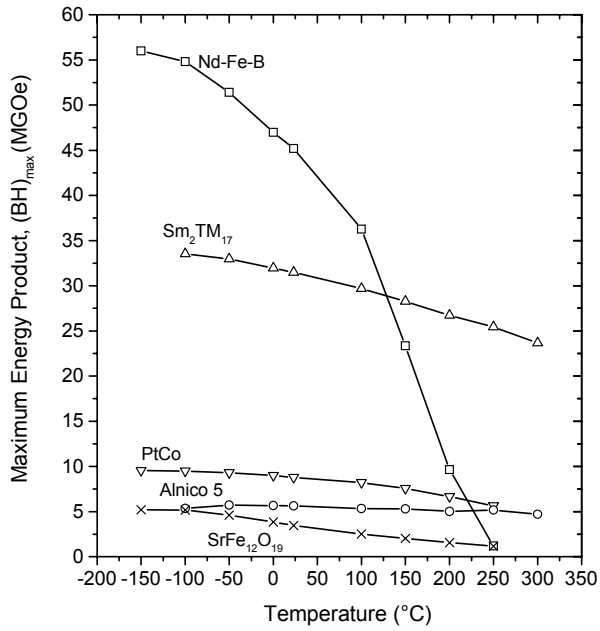


Figure 1.1. Temperature dependence of $(BH)_{\max}$ for five types of permanent magnets.

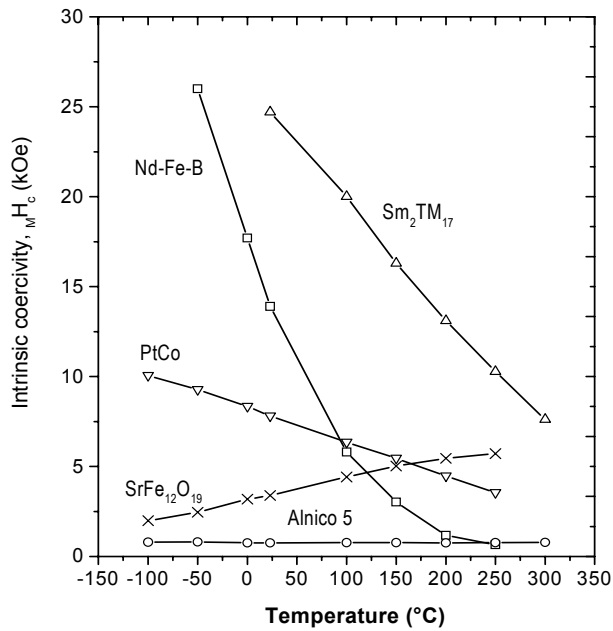


Figure 1.2. Temperature dependence of $M H_c$ for five types of permanent magnets.

Possessing the highest Curie temperature and moderately high magnetization and energy product among the high-performance rare earth permanent magnets, Sm_2TM_{17} magnets are the best conventional high-temperature permanent magnets (Ray and Strnat

1972, Ray 1984, Ray et al. 1992). A conventional $\text{Sm}_2\text{TM}_{17}$ magnet can operate up to 300°C . The problem associated with higher temperature ($> 300^\circ\text{C}$) operation has been that the intrinsic coercivity of these magnets drops sharply with increasing temperature. Upon heating, MH_c of the 2:17 magnets drops sharply from their room temperature values of 20 to 30 kOe (or higher) to only 3 to 6 kOe at 400°C and 1 to 3 kOe at 500°C (Figure 1-3). Low intrinsic coercivity at high temperatures results in nonlinear 2nd-quadrant induction demagnetization curves (B curves) above $\approx 300^\circ\text{C}$. A linear 2nd-quadrant B curve is critical for all dynamic applications, such as for generators and motors.

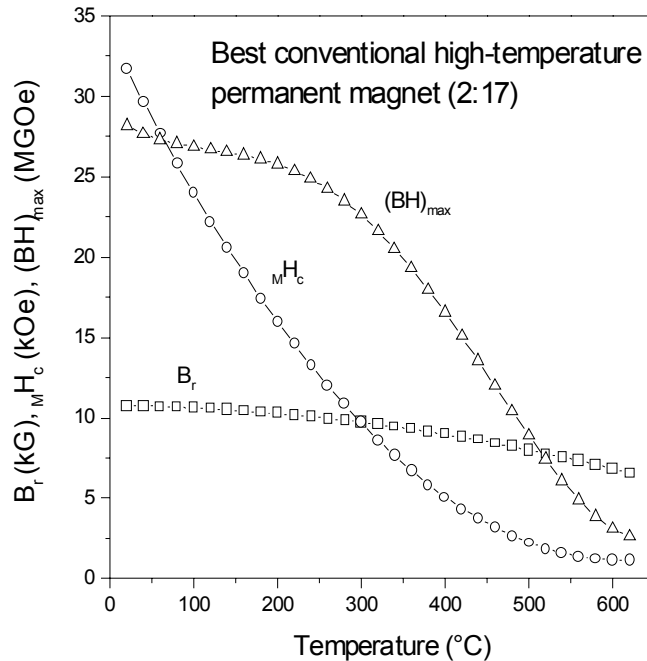


Figure 1-3. Temperature dependence of the best conventional high-temperature 2:17 magnet.

In a dynamic application, the operating point of a magnet keeps cycling. If the intrinsic coercivity is low, then the induction demagnetization curve can be nonlinear. Under this circumstance, the operating point of the magnet can be reduced to below the knee in the induction demagnetization curve and the induction can be significantly reduced irreversibly. If the intrinsic coercivity of the magnet is sufficiently high, then the induction demagnetization curve can be linear. Under this circumstance, the induction will be reversible around the operating point even at a quite low permeance value as shown in Figure 1-4. The maximum operating temperature of a magnet can be defined as the temperature limit at which the induction demagnetization curve of the magnet still maintains the linearity. Therefore, to increase the operating temperature of permanent magnet materials, the key is to increase intrinsic coercivity at high temperature, so that their induction demagnetization curves remain linear at the operating temperature.

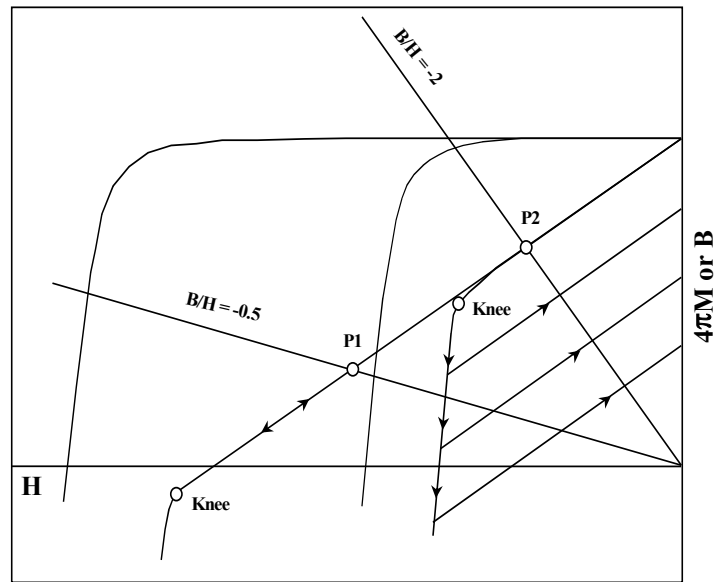


Figure 1-4. Intrinsic coercivity and linearity of an induction demagnetization curve.

2. Candidate alloy system for high-temperature permanent magnet materials

Two criteria of high-temperature permanent magnets are high Curie temperature and high magneto-crystalline anisotropy. At least within the foreseeable future, these requirements can be met probably only in the Sm-Co based system. It is well known that in a rare earth-transition metal (RE-TM) compound, the Curie temperature is primarily determined by the TM sublattice, while the crystalline anisotropy is primarily contributed by the RE sublattice unless at temperatures as high as close to the Curie point. Research on RE-TM compounds has indicated that among all 3d transition metals, Co provides the highest Curie temperature, while among all light rare earths, Sm usually provides the highest crystalline anisotropy. One exception is the cubic Laves 1:2 compounds for which the Fe compounds have higher Curie temperature than the Co compounds.

Figure 2-1 shows Curie temperature, T_C , versus Co content in Sm-Co binary compounds. In this figure, Curie temperature data for LaCo_{13} and $\text{Sm}_2\text{Co}_{14}\text{B}$ are also included. It can be seen from Figure 2-1 that there exists an almost linear relationship between the Curie temperature and the Co content: the higher the Co content in a compound, the higher the Curie temperature of the compound, which clearly demonstrates the importance of the Co content to the Curie temperature. Figure 2-2 illustrates the dependence of the anisotropy field, H_A , on individual rare earth in binary RECo_5 compounds with RE = Y, La, Ce, Pr, Nd, Sm, and MM. It is obvious that the SmCo_5 compound has the highest anisotropy field. Figure 2-3 shows the dependence of

anisotropy field, H_A , on individual rare earth in binary RE_2Co_{17} compounds with $RE = Y, Ce, Pr, Nd, \text{ and } Sm$. It is interesting that in all of the 2:17 compounds, only Sm_2Co_{17} has uniaxial magneto-crystalline anisotropy and, therefore, possesses a large crystalline anisotropy field. Sm even behaves uniquely in ternary $RE_2Fe_{14}B$ compounds. The magneto-crystalline constant K_1 of $Sm_2Fe_{14}B$ is a negative value as shown in Figure 2-4. This means that the easy magnetization direction for $Sm_2Fe_{14}B$ is in the basal plane rather than along the c -axis, such as in the case for $RE = Y, Ce, Pr, \text{ and } Nd$. However, the absolute value of K_1 for $Sm_2Fe_{14}B$ is the largest, which means that there exists the largest magneto-crystalline anisotropy between the basal plain and the c -axis for $Sm_2Fe_{14}B$.

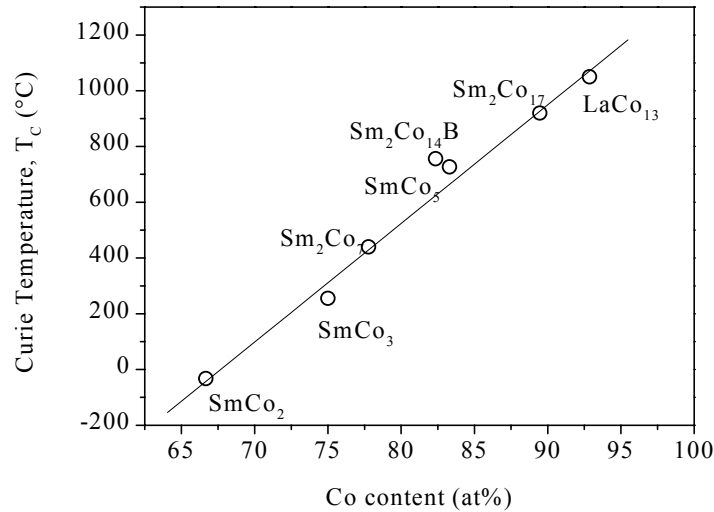


Figure 2-1. Curie temperature, T_c , versus Co content in Sm-Co binary compounds. Data for $LaCo_{13}$ and $Sm_2Co_{14}B$ are also included.

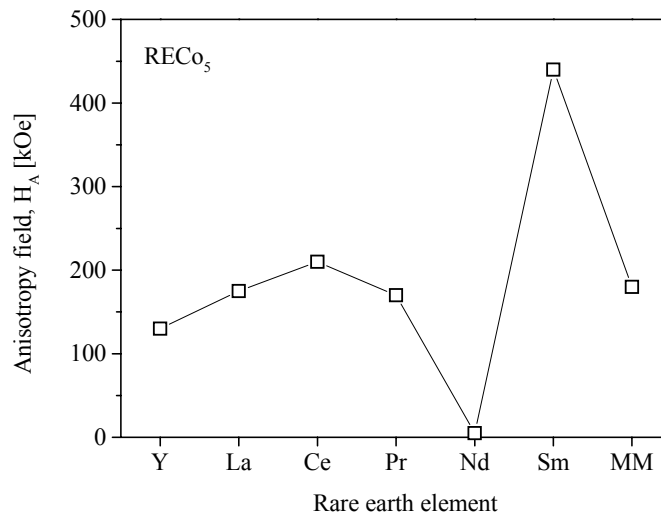


Figure 2-2. Anisotropy field, H_A , in binary $RECo_5$ compound.

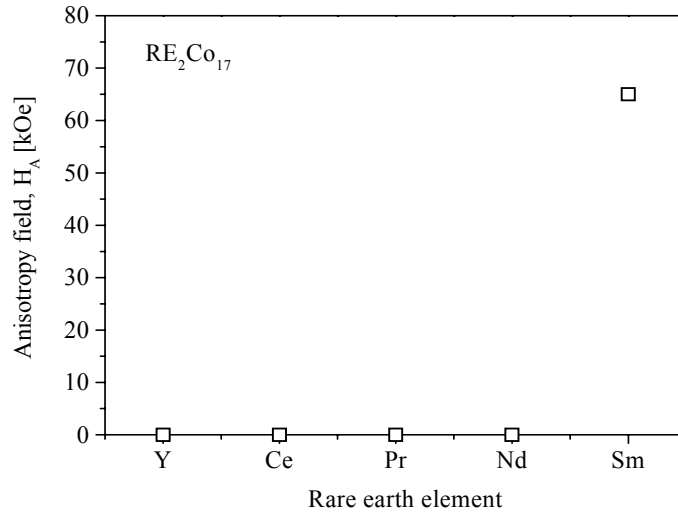


Figure 2-3. Anisotropy field, H_A , in binary RE_2Co_{17} compound.

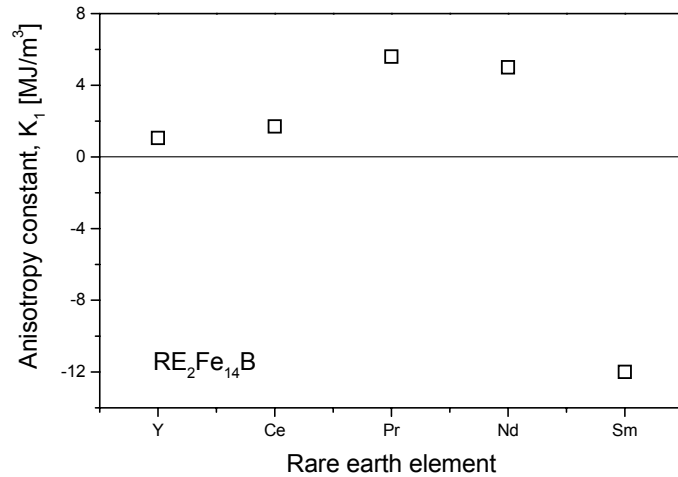


Figure 2-4. Anisotropy constant K_1 in $RE_2Fe_{14}B$ ternary compounds

It can be concluded from the above analysis that until a totally new high-temperature permanent magnet material is discovered, an appropriate approach to developing better high-temperature permanent magnet materials that satisfy the requirements of the advanced power devices is to significantly improve the conventional Sm-Co type magnets, especially $Sm_2(Co,Fe,Cu,Zr)_{17}$ magnets and to develop new compounds based on Sm-Co compounds. In order to satisfy high-temperature ($> 400^\circ C$) applications, the new materials have to possess high intrinsic coercivity at high temperatures ($> 400^\circ C$) so that the induction demagnetization curve remains linear at the operating temperature. Under this condition, the irreversible loss of magnetization caused by high temperature can be minimized.

3. New Sm₂Co₁₇-type high-temperature permanent magnet materials

In recent years, extensive research has been carried out to substantially improve the high-temperature performance of the Sm-TM permanent magnets and a breakthrough was made in 1999. As a result of this breakthrough, the maximum operating temperature of permanent magnets has been increased from around 300°C to as high as 550°C. This advance was made on systematic studies of the effects of compositions on the high-temperature intrinsic coercivity of Sm-TM type of permanent magnets.

3.1 Effects of compositions on high-temperature intrinsic coercivity of Sm-TM permanent magnets

3.1.1 Effect of Sm on high-temperature intrinsic coercivity of Sm-TM permanent magnets

The Sm content, or the z value, in Sm(Co,Fe,Cu,Zr) _{z} , strongly affects the intrinsic coercivity of Sm₂(Co,Fe,Cu,Zr)₁₇-type of permanent magnets. As early as in 1982, S. Liu et al. (Liu et al. 1982) determined the temperature dependence of a few SmCo₅ and Sm₂TM₁₇ permanent magnets up to 750°C. They observed that a magnet specimen of SmTM₇ that had a smaller z value of 7 (higher Sm content) possessed higher intrinsic coercivity than a magnet specimen of SmTM_{7.43} that had a larger z value of 7.43 at high temperatures. More recently, A.S. Kim (Kim, 1998) observed that a SmTM₇ magnet had a much lower temperature coefficient of coercivity than a SmTM₈ magnet. With a high Sm content (low z value) in the magnet, an intrinsic coercivity of 5 kOe was achieved at 500°C. J.F. Liu et al. (Liu et al. 1999) studied the high-temperature magnetic properties of SmTM _{z} with $z = 6.7 - 9.1$ at temperatures up to 500°C. They found that the lower z value led to a smaller temperature coefficient of intrinsic coercivity. When z changed from 7.0 to 8.5, the temperature coefficient of intrinsic coercivity changed from $-0.03\%/^{\circ}\text{C}$ to $-0.25\%/^{\circ}\text{C}$.

When dealing with the effect of Sm content or z value, it is important to realize that not all Sm exists in the Sm-TM compounds in sintered Sm₂(Co,Fe,Cu,Zr)₁₇-type of magnets. A small amount of Sm exists in the form of Sm₂O₃, because Sm is a very active element, and some Sm is oxidized during the fine-powder processing and oxide formation. Under normal conditions, a sintered Sm₂(Co,Fe,Cu,Zr)₁₇ magnet contains 0.3 – 0.6 wt% oxygen. It is easy to understand that oxygen reduces the effective Sm content by 6.27 times the weight fraction of the oxygen. This means that for each 0.1 wt% oxygen there will be 0.627 wt% Sm to be consumed and reacted with oxygen. Therefore, it is useful to define an effective z value that represents the atomic ratio of the transition metals over the metallic part of Sm. Table 3-1 shows the effective z in Sm(Co_{0.8}Fe_{0.1}Cu_{0.08}Zr_{0.02})_{7.0} with differing oxygen contents. These data were calculated under an assumption that all oxygen in sintered Sm-TM magnets exists as Sm₂O₃ and it is believed that Zr is more likely to react with C in the alloy and form ZrC rather than ZrO

(Liu, S. et al. 1999). It can be seen from Table 3-1 that when the oxygen content increases from 0 wt% to 0.60 wt%, the effective z value changes from 7.00 to 8.16. Therefore, stating a nominal z in rare earth permanent magnets without simultaneously mentioning the oxygen content in the magnet is not very meaningful. The z values given in this chapter are the effective z unless otherwise specified.

Table 3-1. Oxygen content and effective z in $\text{Sm}(\text{Co,Fe,Cu,Zr})_7$

| O [wt%] | 0.00 | 0.20 | 0.40 | 0.60 | 0.80 | 1.00 |
|-------------|------|------|------|------|------|------|
| Effective z | 7.00 | 7.35 | 7.73 | 8.16 | 8.64 | 9.17 |

Generally speaking, decreasing the z value (increasing the Sm content) of the conventional 2:17 magnets results in decreased intrinsic coercivity at room temperature, but increased intrinsic coercivity at high temperatures. Figure 3-1 summarizes the effect of z value on M_{H_c} of $\text{Sm}(\text{Co}_{0.795}\text{Fe}_{0.09}\text{Cu}_{0.09}\text{Zr}_{0.025})_z$ (Liu, S. et al.2000a). Both effective and nominal z values are given in this figure. The effective z value in most conventional 2:17 magnets is approximately 8.3 - a value much higher than all magnets presented in this figure. It can be seen from Figure 3-1 that M_{H_c} at room temperature is very sensitive to the z value and M_{H_c} increases rapidly with increasing z. As the temperature rises, especially when $T \geq 500^\circ\text{C}$, M_{H_c} becomes less sensitive to z. It can be seen that there is a peak (denoted by pk) in each M_{H_c} -z curve in the temperature range of 300-500°C. It is interesting to note that as the temperature increases, the z value corresponding to the peak M_{H_c} shifts toward lower values of z. As shown in Figure 3-2, the effective z values corresponding to the peak M_{H_c} at 300, 450, and 500°C are 7.86, 7.62, and 7.38, respectively. It is obvious that at room temperature, the peak should occur at $z \geq 8.10$, while at 550 and 600°C, the peaks should occur at $z \leq 7.14$.

It can also be concluded from Figure 3-1 that M_{H_c} becomes more and more sensitive to temperature with increasing z. This trend can be seen more clearly from Figure 3-2, which shows the temperature dependence of M_{H_c} for $\text{Sm}(\text{Co}_{0.795}\text{Fe}_{0.09}\text{Cu}_{0.09}\text{Zr}_{0.025})_z$. It can be seen from Figure 3-2 that when the effective z = 7.14, the coercivity slightly increases with increasing temperature in the temperature range from 300 to 450°C. As z increases, M_{H_c} gradually increases in the temperature range of 300 – 450°C and displays increased negative temperature coefficients of M_{H_c} . When z exceeds 7.86, M_{H_c} decreases with z at the entire temperature range from 300 to 600°C.

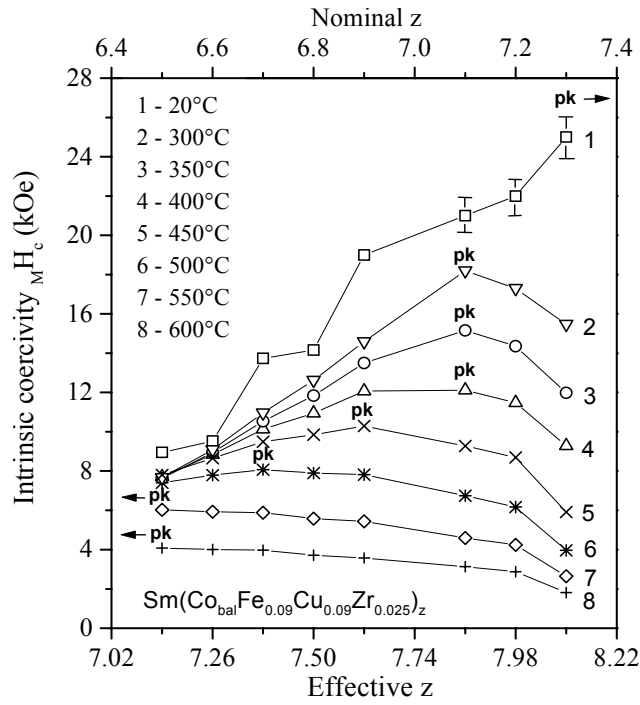


Figure 3-1. Dependence of intrinsic coercivity of $\text{Sm}(\text{Co}_{0.795}\text{Fe}_{0.09}\text{Cu}_{0.09}\text{Zr}_{0.025})_z$ on z value at various temperatures.

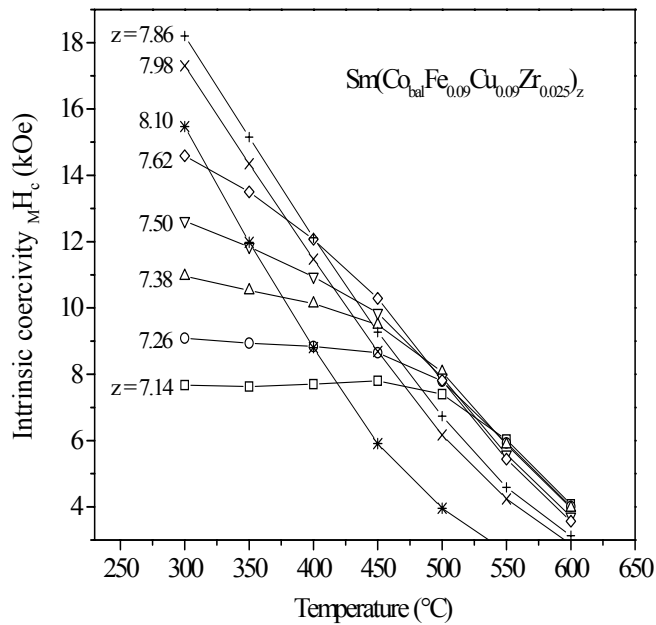


Figure 3-2. Temperature dependence of intrinsic coercivity for $\text{Sm}(\text{Co}_{0.795}\text{Fe}_{0.09}\text{Cu}_{0.09}\text{Zr}_{0.025})_z$ from 300 to 600°C.

3.1.2 Effect of Fe on High Temperature MH_c of Sm-TM Magnets

Fe also has strong effect on high-temperature coercivity of $Sm_2(Co,Fe,Cu,Zr)_{17}$ -type permanent magnets. Increasing Fe content in 2:17 type magnets effectively enhances their saturation magnetization and maximum energy product. However, it was observed in the mid-1990s that high Fe content (or low Co content) resulted in poor high-temperature stability of the magnets (Liu and Hoffman, 1996, Ma et al. 1996, Liu et al. 1997). In 1998, C.H. Chen et al. (Chen, et al. 1998) obtained sintered $Sm_2(Co,Fe,Cu,Zr)_{17}$ -type permanent magnets with improved high-temperature performance by reducing the Fe content in the magnet alloys. A high intrinsic coercivity of 8.3 kOe at 400°C was achieved when the Fe content was decreased to 7 wt%. Their 2:17 magnets with low Fe content demonstrated lower irreversible loss of magnetic flux, higher maximum energy product, and lower temperature coefficient of intrinsic coercivity as compared with the conventional 2:17 magnets that contain 15-20 wt% Fe. In 1999, J.F. Liu (Liu et al. 1999) accomplished intrinsic coercivity of 10.7 kOe at 500°C in a cast magnet alloy.

Generally speaking, decreasing Fe content (increasing Co content) in the 2:17 magnets does not strongly affect their room temperature coercivity, but significantly enhances their coercivity at high temperatures. The effect of Fe content on intrinsic coercivity in $Sm(Co_{bal}Fe_vCu_{0.09}Zr_{0.03})_{7.5}$ at high temperatures from 400°C to 600°C is given in Figure 3-3 (Liu, S. et al. 2000c). It should be noted that the Fe content in conventional 2:17 magnets is $v = 0.21 - 0.31$, much higher than the Fe content in magnet materials in this figure. It can be seen from Figure 3-3 that the high-temperature MH_c increases rapidly with decreasing Fe content in the magnet alloys. At 400°C, MH_c increases from 5.6 kOe when $v = 0.22$ to 12.7 kOe when $v = 0.1$. A coercivity peak appears when $v = 0.1$ at 400°C. This peak shifts to $v = 0.07$ at higher temperatures.

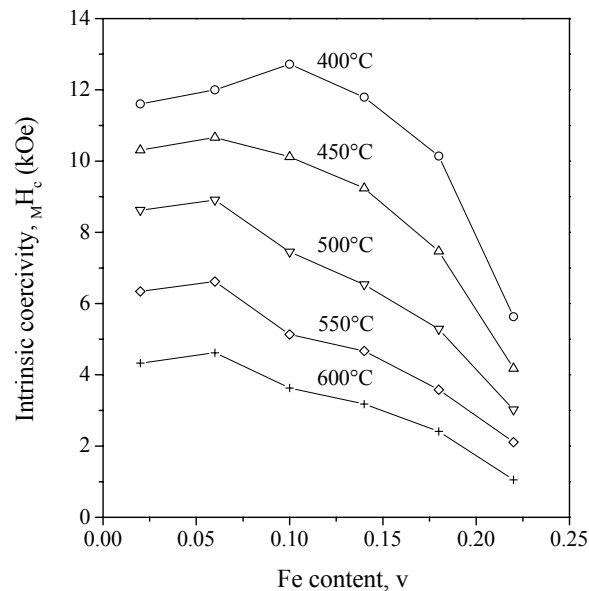


Figure 3-3. High-temperature intrinsic coercivity, MH_c , as a function of Fe content, v , in $Sm(Co_{bal}Fe_vCu_{0.09}Zr_{0.03})_{7.5}$.

3.1.3. Effect of Cu on High Temperature MH_c of Sm-TM Magnets

It is well known that coercivity in the $Sm_2(Co,Fe,Cu,Zr)_{17}$ type of magnets originates from the pinning of the domain wall in the Cu-rich cell boundary phase in a fine-scaled cellular microstructure (Livingston and martin, 1977, Mishra et al. 1981, Ray et al. 1987). Therefore, sufficient Cu content is essential to develop high coercivity at both room temperature and high temperatures. Generally speaking, MH_c increases with the Cu content monotonously. However, the effect of Cu on increasing MH_c is quite different at different temperatures. Figure 3-4 shows the temperature dependence of intrinsic coercivity for $Sm(Co_{bal}Fe_{0.1}Cu_xZr_{0.025})_{6.7}$. It was observed that when a magnet contains very low Cu, its MH_c could have a positive temperature coefficient. This abnormal temperature dependence of intrinsic coercivity is explained in Section 3.6.

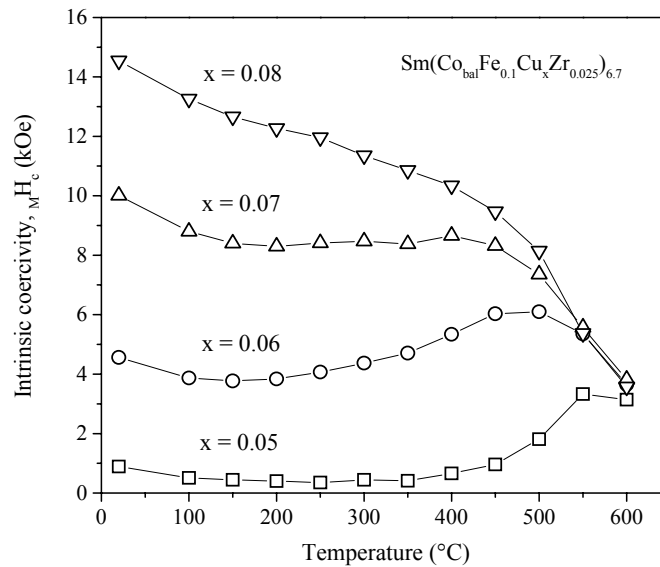


Figure 3-4. Temperature dependence of intrinsic coercivity for $Sm(Co_{bal}Fe_{0.1}Cu_xZr_{0.025})_{6.7}$.

3.1.4. Effect of Zr on High Temperature MH_c of Sm-TM Magnets

Zr has an important effect on the development of coercivity in the $Sm_2(Co,Fe,Cu,Zr)_{17}$ type magnets. It has been observed that Zr is critical in developing high coercivity at both low and high temperatures. It was observed that intrinsic coercivity rapidly increased with increasing Zr and a peak coercivity value was reached at an optimum Zr content. The squareness of the 2nd quadrant demagnetization curve is strongly dependent on Zr content in magnet alloys. The knee field is rapidly enhanced with increasing Zr content. Figure 3-5 shows the effect of the Zr content on the high-temperature intrinsic coercivity in $Sm(Co_{bal}Fe_{0.09}Cu_{0.08}Zr_y)_{7.62}$. It is obvious that when

the Zr content is lower than $y = 0.01$, the coercivity is very low at all temperatures. The coercivity is substantially enhanced when the Zr content increases to $y = 0.018$. It is also seen from this figure that coercivity peaks appear for 300, 350, 400 and 450°C when $y = 0.026$. As temperature is higher than 450°C, magnets containing more Zr display slightly higher coercivity.

The effects of other transition metals such as Ti, Hf, Nb, V, Ta, Cr, and Ni on the high-temperature coercivity of the $\text{Sm}_2(\text{Co}, \text{Fe}, \text{Cu}, \text{Zr})_{17}$ were also investigated. All these elements decreased magnetization. Only Nb demonstrated the effect of slightly enhanced coercivity at high temperatures.

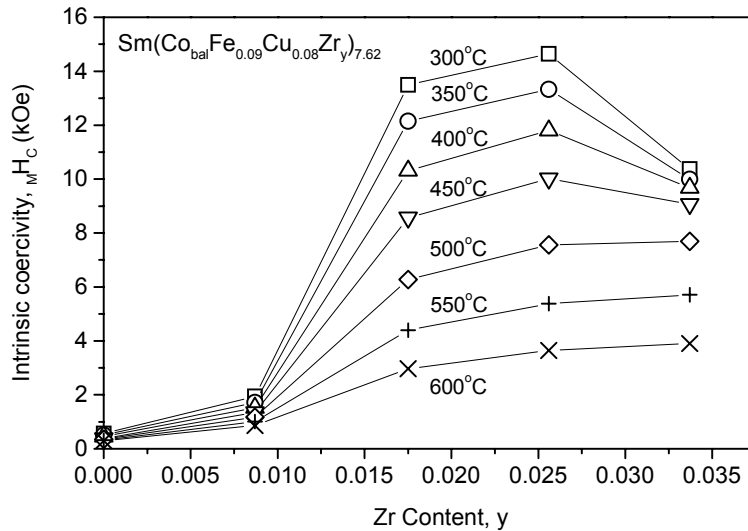


Figure 3-5. Effect of Zr content on high-temperature intrinsic coercivity in $\text{Sm}(\text{Co}_{\text{bal}}\text{Fe}_{0.09}\text{Cu}_{0.08}\text{Zr}_y)_{7.62}$.

3.2. Magnetic properties of new $\text{Sm}_2\text{Co}_{17}$ -based high-temperature permanent magnet materials

The above-mentioned research on the effects of compositions on high temperature performance of the 2:17 type of permanent magnets has resulted in a new series of sintered permanent magnets with significantly improved high-temperature performance accomplished by significantly reducing the Fe content, increasing the Sm content, and adjusting the Cu and Zr contents in the magnet alloys.

The operating temperature of these magnets has been increased from the previous 300°C for conventional high-temperature magnets to as high as 550°C. The M_{Hc} of these new magnets reached 13 kOe at 400°C (two to three times higher than conventional magnets) and 9 kOe at 500°C (four to nine times higher than conventional magnets). The B curves of the new magnets remain linear up to 550°C (250 to 350°C higher than conventional magnets). The temperature coefficients of M_{Hc} for the new magnets can range from a small negative value (-0.03%/°C), to near zero, or they may even be positive (up to +0.3%/°C). As a comparison, the temperature coefficients of M_{Hc} for conventional

SmCo_5 , $\text{Sm}_2\text{TM}_{17}$, and $\text{Nd}_2\text{Fe}_{14}\text{B}$ magnets around room temperature are $-0.3\%/^\circ\text{C}$, $-0.3\%/^\circ\text{C}$, and $-0.9\%/^\circ\text{C}$, respectively.

Figure 3-6 shows the demagnetization curves of $\text{Sm}(\text{Co}_{\text{bal}}\text{Fe}_{0.09}\text{Cu}_{0.09}\text{Zr}_{0.03})_{7.69}$ at 400, 450, and 500°C (Liu, S. et al. 1999a). This magnet illustrates much higher $M\text{H}_c$ and better squareness of demagnetization curves at high temperatures than the conventional 2:17 magnets. Figure 3-7 compares induction demagnetization curves at high temperatures up to 550°C for the best conventional high-temperature 2:17 magnet and the new high-temperature magnets (Walmer 2000b). It can be seen from Figure 3-7 that the best conventional high-temperature 2:17 magnet remains a linear induction demagnetization curve up to 330°C. At 400°C, the induction demagnetization curve is severely bent and a knee appears, while the induction demagnetization curves for the new high-temperature magnets remain linear up to 550°C. Figure 3-8 shows demagnetization curves for a new high-temperature magnet with its maximum operating temperature $T_M = 500^\circ\text{C}$. These new magnets are now commercially available from Electron Energy Corporation.

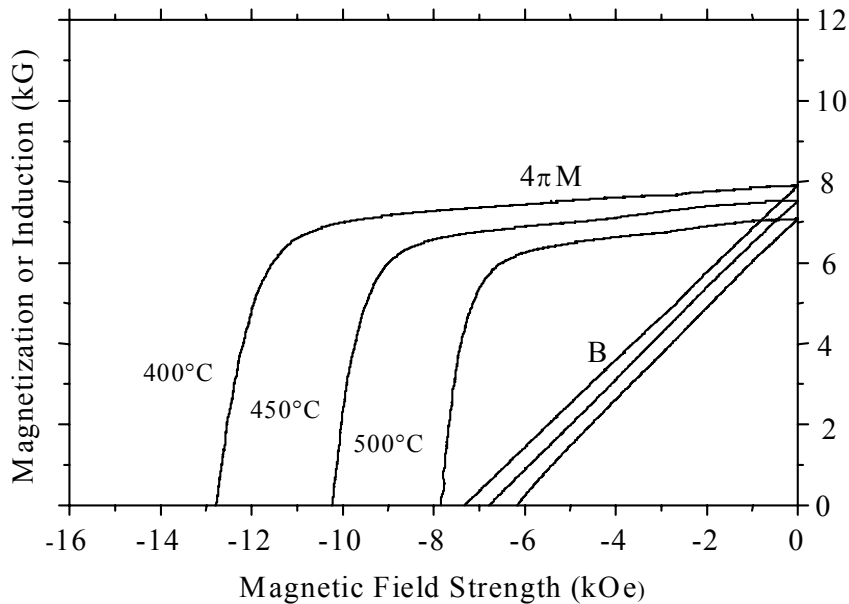
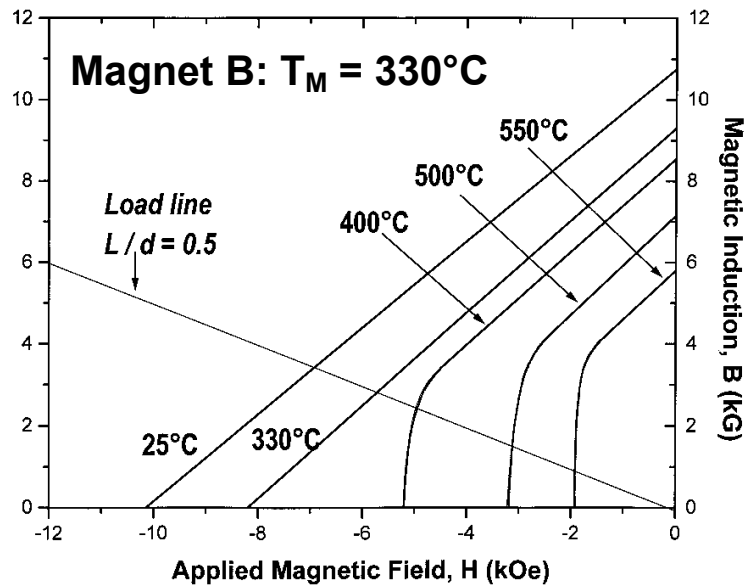
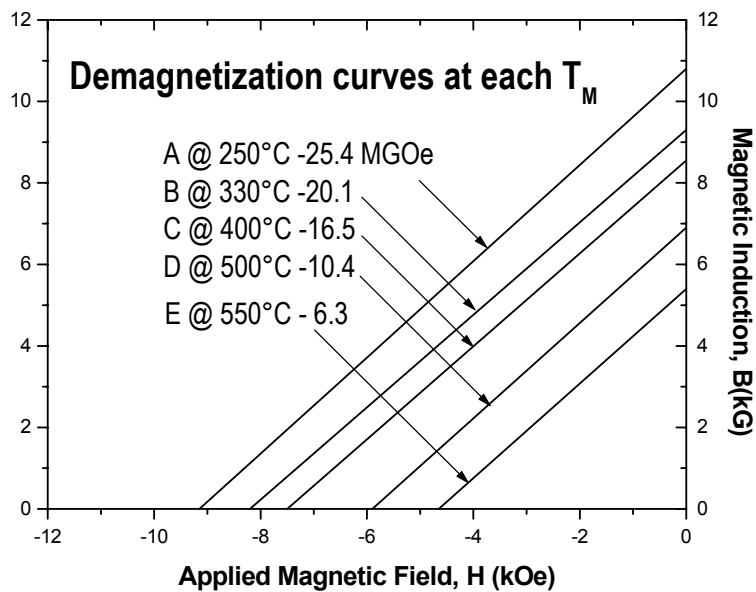


Figure 3-6. Demagnetization curves of $\text{Sm}(\text{Co}_{\text{bal}}\text{Fe}_{0.09}\text{Cu}_{0.09}\text{Zr}_{0.03})_{7.69}$ at 400°C, 450°C, and 500°C.



(a)



(b)

Figure 3-7. Induction demagnetization curves at high temperatures up to 550°C for conventional 2:17 (a) and new high-temperature magnets (b).

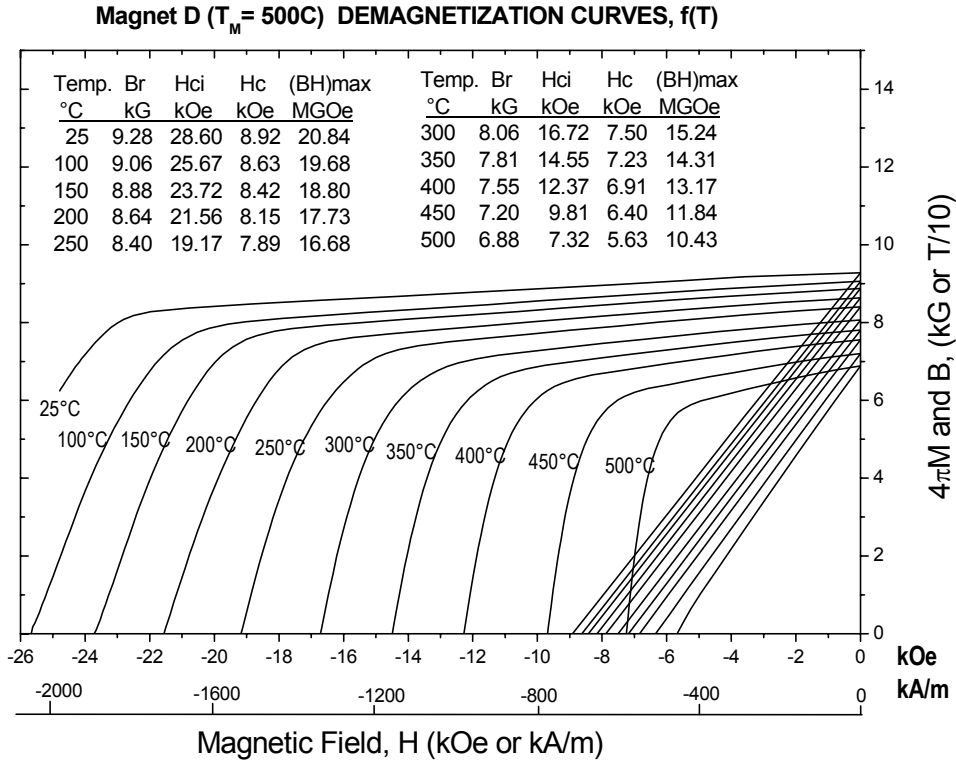


Figure 3-8. Demagnetization curves of a new high-temperature magnet with T_M = 500°C

The temperature dependence of MH_c for some newly-developed sintered Sm-Co based permanent magnets is shown in Figure 3-9 (Liu, S. et al. 2000b). For comparison, the temperature dependence of MH_c of a high-coercivity type of conventional 2:17 magnet is also shown as Curve 1 in the figure. It can be seen from Figure 3-7 that the MH_c of the new magnets is much less temperature sensitive in comparison with the conventional 2:17 magnet. At temperatures above 100°C, the MH_c of $\text{Sm}(\text{Co}_{\text{bal}}\text{Fe}_{0.09}\text{Cu}_{0.09}\text{Zr}_{0.03})_{7.69}$ (Curve 2) is higher than that of the conventional 2:17 magnet. At 400°C, the MH_c is three times higher than that of the conventional magnet. Curve 4 has a very flat portion at a quite high coercivity level from 200 to 400°C. From room temperature to 450°C, the MH_c of $\text{Sm}(\text{Co}_{\text{bal}}\text{Fe}_{0.09}\text{Cu}_{0.09}\text{Zr}_{0.025})_{7.14}$ remains almost constant (Curve 5), making its temperature coefficient very close to zero over this wide temperature range. In addition, a complex temperature dependence of MH_c in some newly-developed magnets was observed (Curve 6). Further details will be presented in Section 3.6.2.

The variation of temperature coefficients of MH_c as a function of temperature for the magnets shown in Figure 3-7 is given in Figure 3-10 (Liu, S. et al. 2000b). As a comparison, Figure 3-10 also gives temperature coefficients of MH_c of a typical SmCo_5 and a Nd-Fe-B magnet. The temperature coefficient of MH_c demonstrated in Figure 3-10 is defined as (Liu, S. et al. 1990b)

$$\beta = \frac{d(MH_c)}{dT} \times \frac{100}{MH_c} \quad (\%/^{\circ}\text{C}). \quad (1)$$

Detailed information about this definition and its calculation will be given in Section 4.

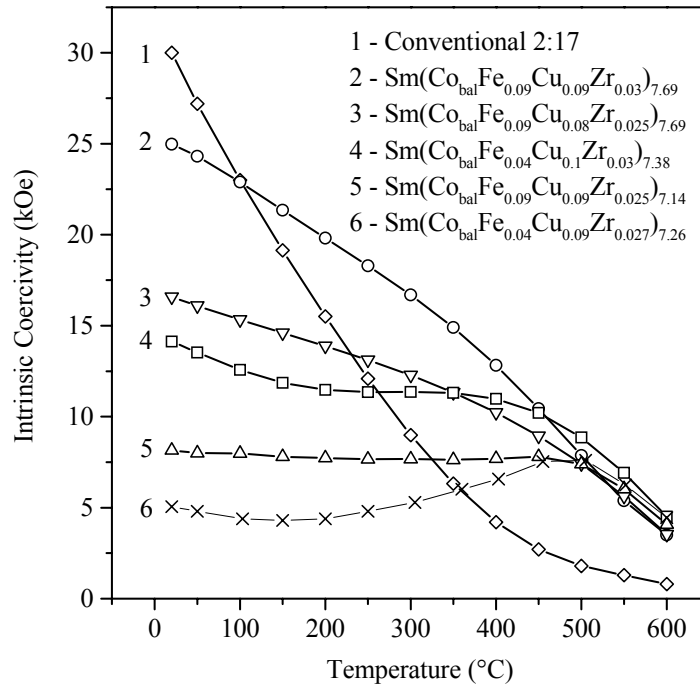


Figure 3-9. Temperature dependence of intrinsic coercivity of various Sm(Co,Fe,Cu,Zr)_z magnets.

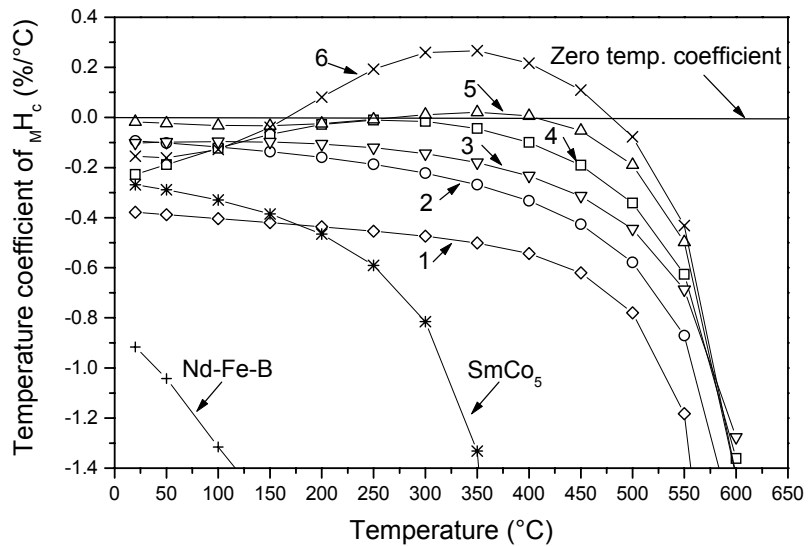


Figure 3-10. Temperature coefficients of various permanent magnets. Numbers (1-6) denote the same magnets as shown in Figure 3-9.

3.3 Dynamic Characterizations of New High-Temperature Permanent Magnets

It is important to realize that the typical magnetic characterization is static. Its results are only meaningful to the static applications in which the operating point of a magnet in the induction demagnetization curve is fixed. Data obtained from a static characterization do not necessarily represent the real capability of a magnet in dynamic applications in which the operating point of the magnet in the induction demagnetization curve is cycled. Examples of dynamic applications are motors, generators, magnetic bearings, and magnetic actuators.

Because these important applications of permanent magnets are dynamic, it is of the utmost importance to know the capability of a magnet under dynamic rather than static conditions. Bearing this in mind, we devised two sets of dynamic characterizations. In the first one, the magnet specimens were magnetically cycled under an applied demagnetizing field of 0 to B_Hc before their magnetic properties were determined. The first set of characterizations was performed from room temperature to 500°C. The second set of characterizations was carried out at a fixed temperature of 400°C with an applied demagnetizing field ranging from 0 to 9 kOe. We compared the dynamic magnetic properties of the new magnets with those of the best conventional 2:17 magnets in these two sets of dynamic characterizations. The maximum operating temperature of the magnet specimens used in these dynamic characterizations is 450°C.

Results of the first set of dynamic characterization are given in Figures 3-11 through 3-14 and summarized in Figure 3-15 (Liu, S. et al. 2000c). It can be seen from these figures that at room temperature, the conventional 2:17 magnets have higher dynamic $(BH)_{max}$. However, at about 250°C, the dynamic $(BH)_{max}$ of the conventional 2:17 magnets begins to sharply decrease. At 400°C, its $(BH)_{max}$ drops to less than 1/20 of the new magnet as shown in Figure 3-13. Results of the second set of dynamic characterizations are summarized in Figure 3-16 (Liu, S. et al. 2000c). It is obvious that the maximum applied demagnetizing field to which the best conventional 2:17 magnet can be subjected without significant loss of $(BH)_{max}$ is about 2 kOe, while for the new magnet it is as high as 8 kOe.

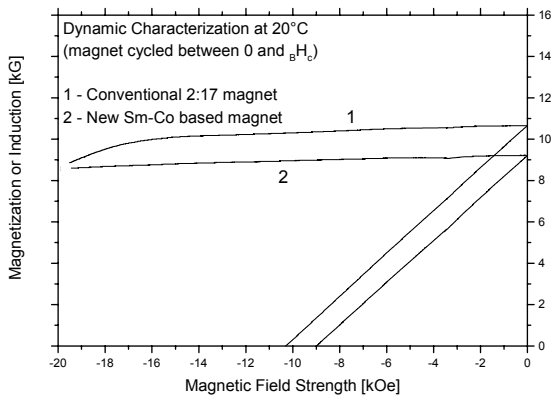


Figure 3-11. Result of dynamic characterization performed at 20°C.

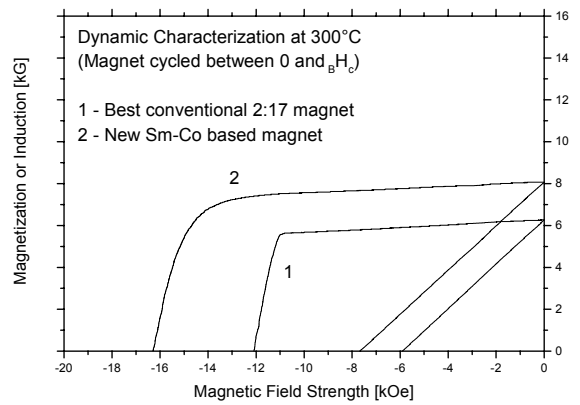


Figure 3-12. Result of dynamic characterization performed at 300°C.

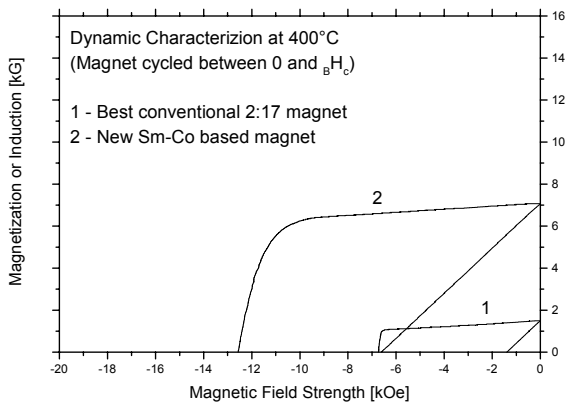


Figure 3-13. Result of dynamic characterization performed at 400°C.

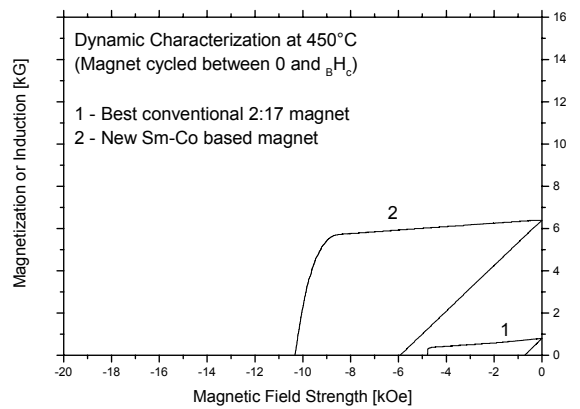


Figure 3-14. Result of dynamic characterization performed at 450°C.

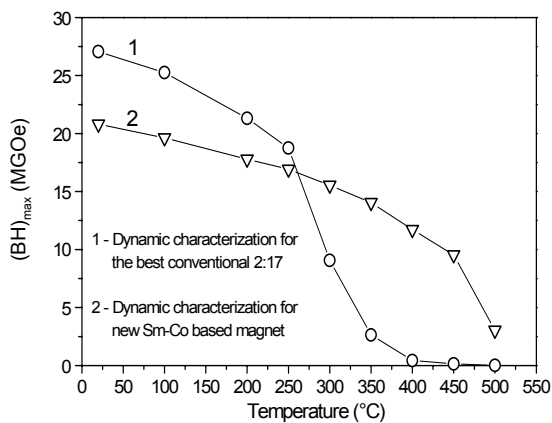


Figure 3-15. A summary of the first set of dynamic characterizations.

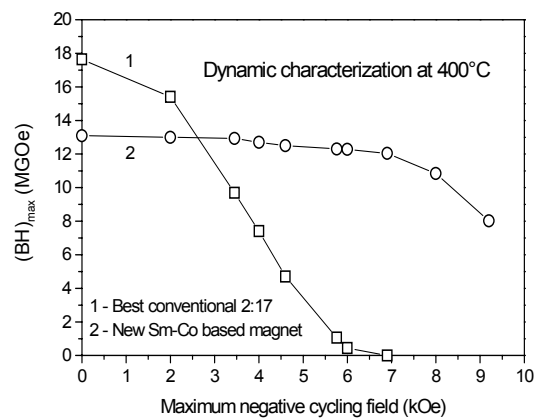


Figure 3-16. A summary of the second set of dynamic characterizations.

3.4 Long-Term Thermal Stability of New High-Temperature Permanent Magnets

An aging experiment was performed to test the long-term high-temperature stability of the new magnets. Figure 3-17 shows the losses of flux density in the first 100 hours for $\text{Sm}(\text{Co}_{0.795}\text{Fe}_{0.09}\text{Cu}_{0.09}\text{Zr}_{0.025})_z$, with effective $z = 7.26, 7.62, 7.86,$ and 8.10 , in a conventional long-term aging experiment performed at 500°C in air. As comparisons, data for a best conventional high temperature 2:17-28 magnet (room temperature $(\text{BH})_{\text{max}} = 28$ MGOe), a conventional 2:17-30 magnet (room temperature $(\text{BH})_{\text{max}} = 30$ MGOe) are also included in the figure. As can be seen from the figure that after aging at 500°C for 100 hours, the flux density losses are about 56% and 36% for the conventional high-temperature 2:17-30 and 2:17-28, respectively. While under the same condition the losses for the best new magnet is only 3% (Liu, S. et al. 2000c).

Figure 3-18 shows the loss of flux density up to 2000 hours for the same magnets. It can be seen from Figure 3-18 that after aging at 500°C for 2000 hours, the flux density losses are 65% and 49% for the conventional high-temperature 2:17-30 and 2:17-28, respectively. Under the same condition the losses for the best new magnet is 19% (Liu, S. et al. 2000a,c).

It is obvious from Figure 3-18 that the newly developed magnets display significantly lower losses of flux density than the conventional 2:17 magnets under the same testing condition. The magnet with $z = 7.62$ gives the best long-term stability. Magnets with the z values lower or higher than 7.62 illustrate relatively larger losses. It is observed that the magnet with $z = 7.26$ displays the largest loss among the four new magnets though at high temperatures it has higher $M\text{H}_c$ than magnets with $z = 7.86$ and $z = 8.10$ (Figure 3-1). This is related to the fact that it has low room temperature $M\text{H}_c$.

Recent study has revealed that the flux density loss of the best high-temperature magnet during the high-temperature in-air aging as shown in Figures 3-17 and 3-18 is caused by the diffusion of Sm to the specimen surface rather than by metallurgical change (Walmer et al. 2000b). Therefore, the loss can be further reduced by applying a proper coating layer.

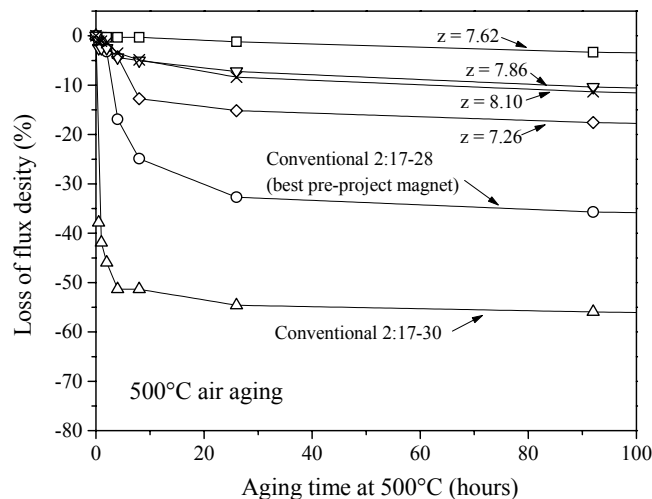


Figure 3-17. Loss of flux density vs. aging time at 500°C for the first 100 hours.

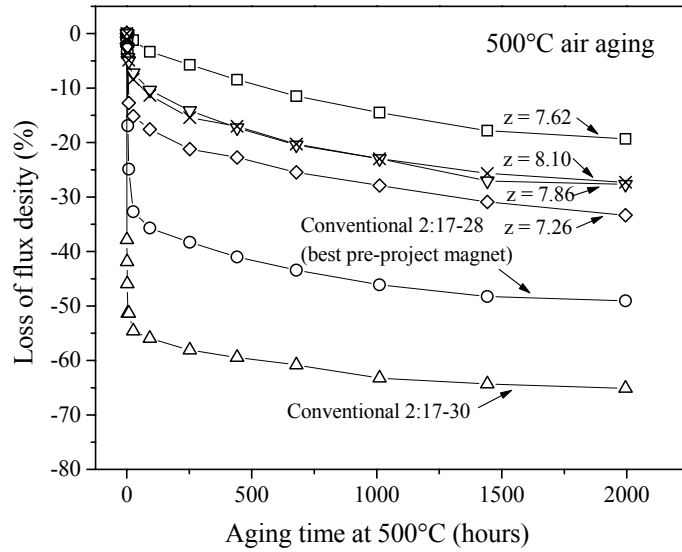


Figure 3-18. Loss of flux density vs. aging time at 500°C up to 2000 hours.

3.5 Microstructure and Crystal Structure

Figure 3-19 is an optical micrograph of $\text{Sm}(\text{Co}_{0.794}\text{Fe}_{0.1}\text{Cu}_{0.09}\text{Zr}_{0.026})_{7.0}$ after aging. The nominal z value of the magnet specimen is 6.46. In other words, the magnet specimen contains very high Sm. Under this condition, it still shows a uniform "one-phase" microstructure. The fine-scaled cellular microstructure of high-temperature magnets has been observed by many researchers. A.S. Kim (Kim, 1998) first observed that the cell size is smaller in a SmTM_7 magnet than in a SmTM_8 magnet. Similar results were reported by J.F. Liu et al. (Liu et al. 1999a), T. Schrefl et al. (Schrefl et al. 2000), and M.S. Walmer et al. (Walmer et al. 2000a,b). Figure 3-20 is a TEM micrograph of a new high-temperature magnet.

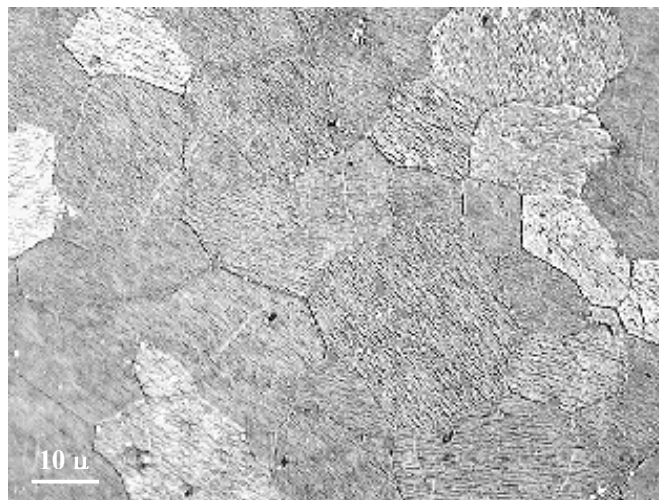


Figure 3-19. Optical micrograph of $\text{Sm}(\text{Co}_{0.794}\text{Fe}_{0.1}\text{Cu}_{0.09}\text{Zr}_{0.026})_{7.0}$ (Nominal $z = 6.46$)

The XRD pattern of $\text{Sm}(\text{Co}_{0.794}\text{Fe}_{0.09}\text{Cu}_{0.09}\text{Zr}_{0.026})_{7.0}$ after solid-solution heat treatment (SSHT) is given in Figure 3-21. This figure suggest that the magnet specimen may have a 1:7 hexagonal crystal structure in the SSHT condition. Figure 3-22 is the XRD pattern of the same magnet after aging and in high coercivity condition. The XRD result indicates that the magnet specimen consists of a 2:17 rhombohedral phase and a 1:5 hexagonal phase. More accurate determination of the crystal structures would rely on addition analyses, including neutron diffraction and Mössbauer work.

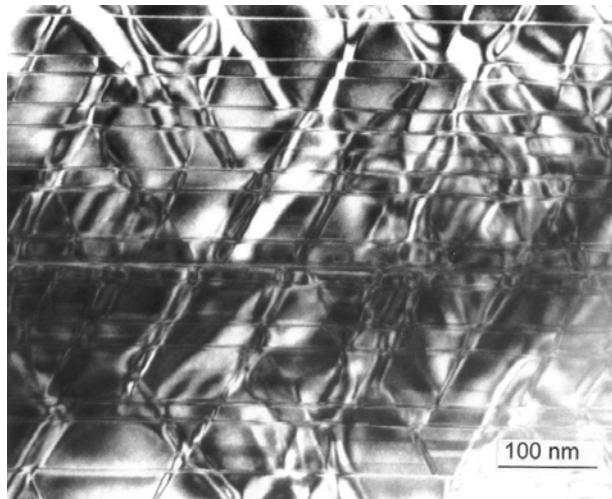


Figure 3-20. TEM micrograph of a new high-temperature magnet.

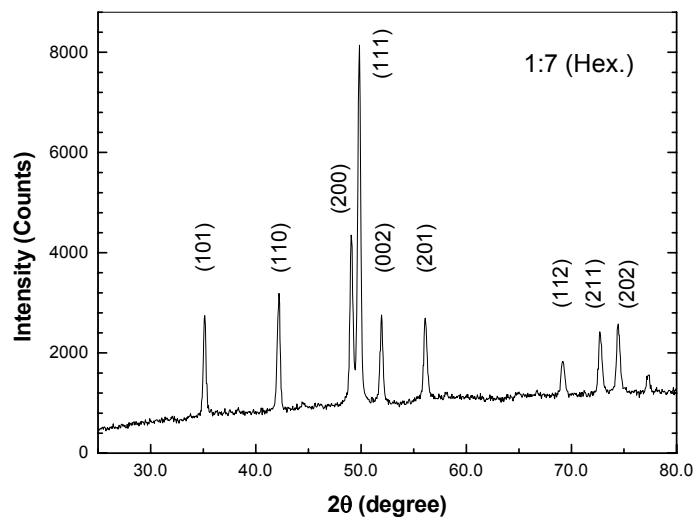


Figure 3-21. XRD pattern of $\text{Sm}(\text{Co}_{0.794}\text{Fe}_{0.09}\text{Cu}_{0.09}\text{Zr}_{0.026})_{7.0}$ after solid solution heat treatment.

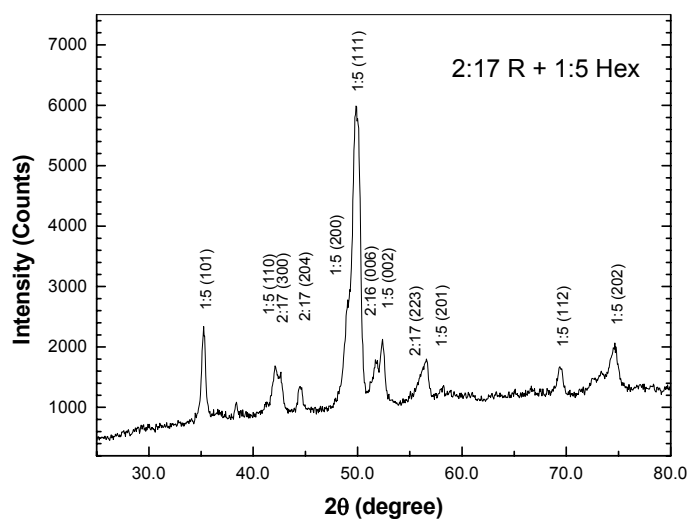


Figure 3-22. XRD pattern of $\text{Sm}(\text{Co}_{0.794}\text{Fe}_{0.09}\text{Cu}_{0.09}\text{Zr}_{0.026})_{7.0}$ after aging.

3.6 Coercivity in $\text{Sm}_2\text{TM}_{17}$ -type permanent magnets

3.6.1 Explanation of effects of Sm, Fe, Cu on intrinsic coercivity

During the development of the new high-temperature permanent magnets, it was observed that Fe, Sm, and Cu contents significantly affect high temperature coercivity of $\text{Sm}_2(\text{Co,Fe,Cu,Zr})_{17}$ -type permanent magnets. Generally speaking, decreasing Fe (increasing Co) content does not strongly affect room temperature coercivity but leads to a significantly higher coercivity at high temperatures; increasing Sm content results in much lower room temperature coercivity but substantially higher coercivity at high temperatures; and increasing Cu content leads to higher coercivity at all temperatures. The effects of Fe, Sm, and Cu on coercivity can be explained by using the temperature dependence of magneto-crystalline anisotropy of the 2:17 cell phase and 1:5 cell boundary phase.

Effects of changing Fe, Sm, and Cu content on element concentrations in the cellular microstructure

It is well known that coercivity in 2:17 magnets originates from the domain wall energy difference between a 1:5 cell boundary phase and a 2:17 cell phase in a fine-scaled cellular microstructure (Livingston and martin, 1977, Mishra et al. 1981, Ray et al. 1987). The 1:5 cell boundary phase has lower crystalline anisotropy K and, in turn, lower domain wall energy E than the 2:17 cell phase. Therefore, domain walls are preferably pinned in the 1:5 cell boundary phase.

Figure 3-23 gives composition maps for a typical high-temperature 2:17 magnet (Liu, S. et al. 2001). It shows a bright field image and concentrations of Zr, Co, Fe, Sm, and Cu, respectively. In the composition maps, a bright region represents a high concentration of an element. It can be clearly seen from Figure 3-23 that the cell interior is rich in Co and Fe, while the cell boundary phase is rich in Sm and Cu.

The Fe content in the 1:5 cell boundary phase of 2:17 magnets containing high Fe content is less than 5 at% (Ray 1990). In contrast, Fe substitution for Co can be made up to 100 at% of Fe in the 2:17 phase (Ray and Strnat 1972). Therefore, it is assumed that changing the Fe content in the 2:17 magnets primarily alters the composition of the 2:17 cell phase. On the other hand, considering the facts that: (i) the SmCo_5 phase has a relatively high solubility for Sm even at low temperature ($<400^\circ\text{C}$) and can be expressed as $\text{SmCo}_{5-\delta}$ with $\delta > 0$ (Khan 1974), which is different from $\text{Sm}_2\text{Co}_{17}$; (ii) most of the Cu in 2:17 magnets is concentrated in the 1:5 cell boundary phase (Ray 1990); and (iii) Cu substitution for Co in SmCo_5 can be made up to 100 at% of Cu (Ray 1990), it is assumed that changing the contents of Sm and Cu primarily affects the composition of the 1:5 cell boundary phase.

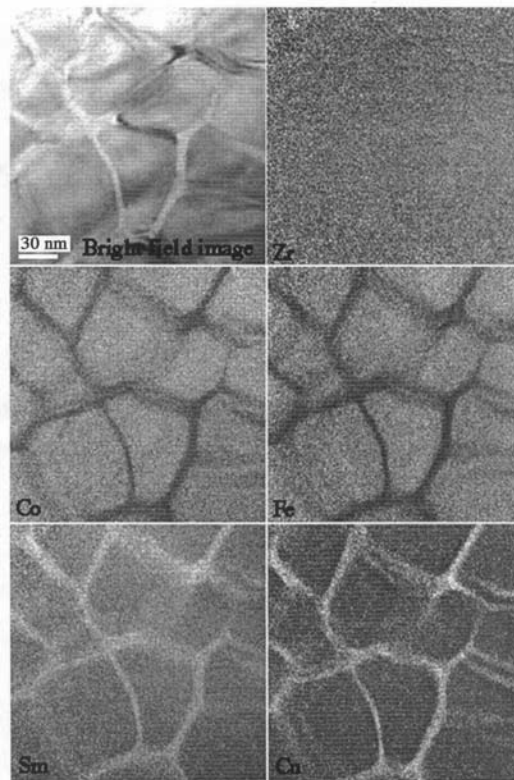


Figure 3-23. Composition map of a high-temperature $\text{Sm}_2(\text{Co,Fe,Cu,Zr})_{17}$ magnet.

Effect of decreasing Fe (increasing Co) content

R.S. Perkins et al. (Perkins et al. 1975) showed that when the Fe substitution for Co was decreased from 40 at% to 20 at%, the room temperature anisotropy field of a 2:17 alloy rapidly increased from 32 kOe to 65 kOe. However, when the Fe content was further decreased from 20 at% to 0, the anisotropy field did not show a significant change. In conventional 2:17 magnets, the Fe content is around 20 at%. The Fe content has been decreased to 0-10 at% in the newly developed high temperature 2:17 magnets. Therefore, it can be concluded that decreasing Fe content does not lead to a significant change of the crystalline anisotropy in the 2:17 cell phase at room temperature (T_m). This is shown in Figure 3-24 which schematically

illustrates the temperature dependence of crystalline anisotropy for the 2:17 cell phase (curve 1) and the 1:5 cell boundary phase (curve 2) in a conventional 2:17 magnet and for the 2:17 cell phase in a 2:17 magnet containing low Fe (curve 3).

On the other hand, decreasing Fe content (increasing Co content) results in a significant increase of Curie temperature of the 2:17 cell phase (Ray and Strnat 1972). Thus, curve 3 should be higher than curve 1 in the high temperature region as shown in Figure 3-24. This explains why decreasing Fe content does not strongly affect room temperature coercivity but leads to a significantly higher coercivity at high temperature.

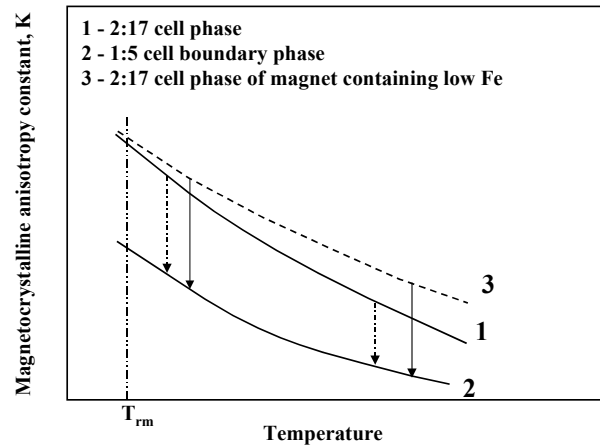


Figure 3-24. Schematic temperature dependence of magneto-crystalline anisotropy for the 2:17 cell phase and 1:5 cell boundary phase in a conventional 2:17 magnet and for the 2:17 cell phase in a 2:17 magnet containing low Fe.

Effect of increasing Sm content

As discussed earlier, when the Sm content in the magnet alloy is increased, the extra Sm primarily enters the cell boundary region. Since the magneto-crystalline anisotropy in Sm-Co compounds mainly originates from the Sm-Sm sublattice, it is reasonable to believe that increasing the Sm content in $\text{Sm}(\text{Co,Cu})_{5-\delta}$ would result in an increased crystalline anisotropy at room temperature, T_{rm} , and at low temperatures.

It is well known that the magnitude of the Curie temperature in Sm-Co compounds is determined by the Co-Co sublattice. Thus, increasing Sm content in $\text{Sm}(\text{Co,Cu})_{5-\delta}$ leads to a decreased Curie temperature of the 1:5 cell boundary phase. From the above analysis, the temperature dependence of the crystalline anisotropy of the 1:5 cell boundary phase in the magnet containing high Sm would be a curve 3 shown in Figure 3-25. It is obvious that at room temperature and low temperature, the magnet containing high Sm displays lower coercivity, while at high temperature, it displays higher coercivity as compared with conventional 2:17 magnets.

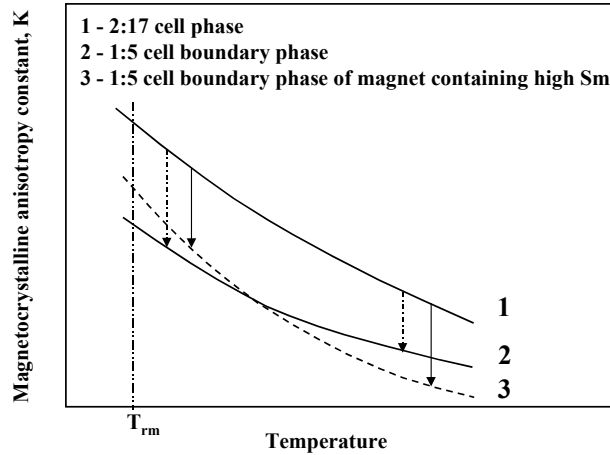


Figure 3-25. Schematic temperature dependence of magneto-crystalline anisotropy constants for the 2:17 cell phase and the 1:5 cell boundary phase in a conventional 2:17 magnet and for 1:5 cell boundary phase in a 2:17 magnet containing high Sm.

Effect of increasing Cu content

When the Cu content in 2:17 magnets is increased, the extra Cu mainly goes to the 1:5 cell boundary $\text{Sm}(\text{Co,Cu})_{5-8}$ phase, resulting in both a decreased crystalline anisotropy and a decreased Curie temperature (Lecrard et al. 1994). This results in a curve 3 of the temperature dependence of crystalline anisotropy of the 1:5 cell boundary phase shown in Figure 3-26. It is then understandable that the magnet containing higher Cu shows higher coercivity at all temperature ranges.

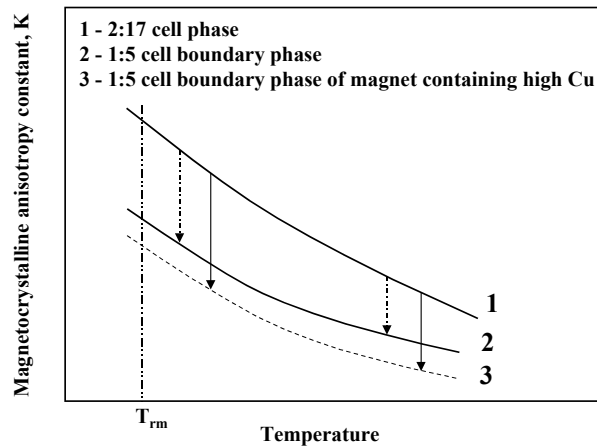


Figure 3-26. Schematic temperature dependence of magneto-crystalline anisotropy constants for the 2:17 cell phase and the 1:5 cell boundary phase in a conventional 2:17 magnet and for the 1:5 cell boundary phase in a 2:17 magnet containing high Cu.

3.6.2 Novel temperature dependence of intrinsic coercivity

Novel temperature dependence of M_Hc was observed during the research on high-temperature permanent magnets in some newly-developed magnets. A positive

temperature coefficient of intrinsic coercivity in SmTM_z with $z = 7$ was reported by J.F. Liu et al. (Liu et al. 1998) in 1998. In 1999, S. Liu et al. (Liu et al. 1999a) observed a complex temperature coefficient in $\text{Sm}(\text{Co}_{\text{bal}}\text{Fe}_{0.04}\text{Cu}_{0.09}\text{Zr}_{0.027})_{7.26}$ that had a low Fe content and a high Cu content. When heating this magnet, MH_c first gradually decreases and reaches a minimum at about 150°C as shown in Figure 3-27. With continued heating, the MH_c of this magnet rapidly increases and forms a maximum at 500°C . The MH_c of this magnet at 500°C is more than 30% higher than its room temperature value. This abnormal temperature variation of MH_c also affects its $(BH)_{\text{max}}$ as shown in Figure 3-28. Another magnet of $\text{Sm}(\text{Co}_{0.825}\text{Fe}_{0.1}\text{Cu}_{0.05}\text{Zr}_{0.025})_{7.38}$ that has low Cu content displays a maximum MH_c at 550°C which is nearly four times higher than its room temperature coercivity value as shown in Figure 3-24. As early as 1990, Russian researchers observed the similar abnormal temperature dependence of coercivity (Popov et al. 1990a,b).

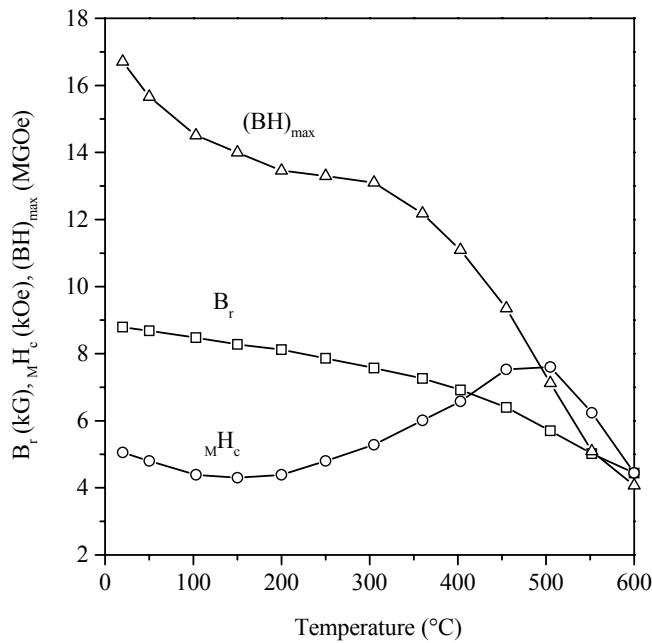


Figure 3.27. Temperature dependence of magnetic properties of $\text{Sm}(\text{Co}_{\text{bal}}\text{Fe}_{0.04}\text{Cu}_{0.09}\text{Zr}_{0.027})_{7.26}$

The novel temperature dependencies of MH_c observed in the new high-temperature magnets as shown in Figures 3-27, 3-28 and in Figure 3-9 (especially magnets 5 and 6) challenge previous coercivity theories. In these theories, the effect of temperature on coercivity is related only to the basic magnetic parameters, such as saturation magnetization and crystalline anisotropy and, thus, the novel temperature dependence of MH_c cannot be explained. Therefore, a new coercivity model is required and this model will certainly lead to a better understanding of the coercivity origin in rare earth permanent magnets.

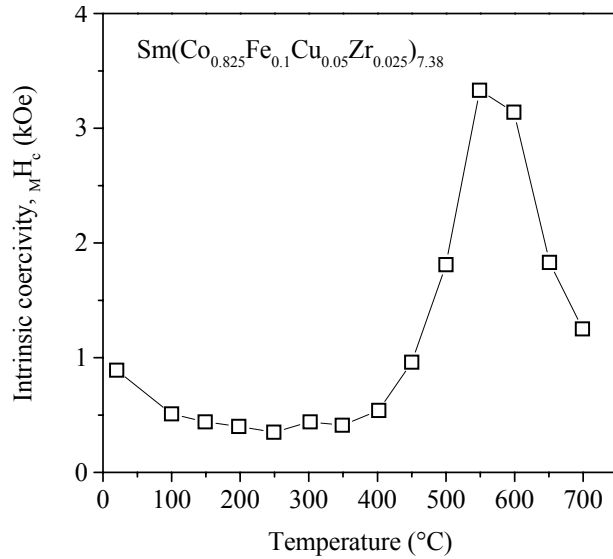


Figure 3.28. Temperature dependence of intrinsic coercivity of $\text{Sm}(\text{Co}_{0.825}\text{Fe}_{0.1}\text{Cu}_{0.05}\text{Zr}_{0.025})_{7.38}$ magnet.

Coercivity mechanisms in permanent magnets are very complicated and many factors affect the coercivity development. However, the complex temperature dependence of MH_c shown in Figures 3-27 and 3-28 clearly suggests that there must be two conflicting coercivity mechanisms that control the coercivity of the magnet. The first mechanism results in higher coercivity at higher temperature, while the second mechanism leads to lower coercivity at high temperature. As a result of these two conflicting mechanisms, a more or less U shaped MH_c versus T curve forms at 20-500°C.

Mechanism I – Domain wall pinning

As mentioned previously, the coercivity in 2:17 type magnets originates from domain wall pinning in the Sm- and Cu-rich 1:5 cell boundary phase of a fine-scaled cellular microstructure. This is because the cell boundary phase has a lower crystalline anisotropy constant K and, in turn, lower domain wall energy E than the 2:17 cell phase. The magnitude of coercivity is determined by the domain wall energy difference between the 1:5 and 2:17 phases. Therefore, higher coercivity at higher temperature implies that the energy difference between the two phases increases with increasing temperature.

Because the Sm- and Cu-rich 1:5 cell boundary phase has not only a lower crystalline anisotropy, but also a lower Curie temperature than the 2:17 cell phase, the crystalline anisotropy of the 1:5 phase may decrease more rapidly upon heating than the 2:17 phase, which may result in the temperature dependencies of crystalline anisotropy of the 1:5 and 2:17 phases resembling the curves in Figure 3-29. It can be seen from Figure 3-29 that as temperature increases, the anisotropy difference between the two phases also increases. This leads to a higher MH_c at higher temperature. It should be noted that while the pinning mechanism may lead to higher coercivity at higher temperatures, it may also lead to lower coercivity at higher temperatures depending on the individual temperature dependence of the 2:17 cell phase and the 1:5 cell boundary phase.

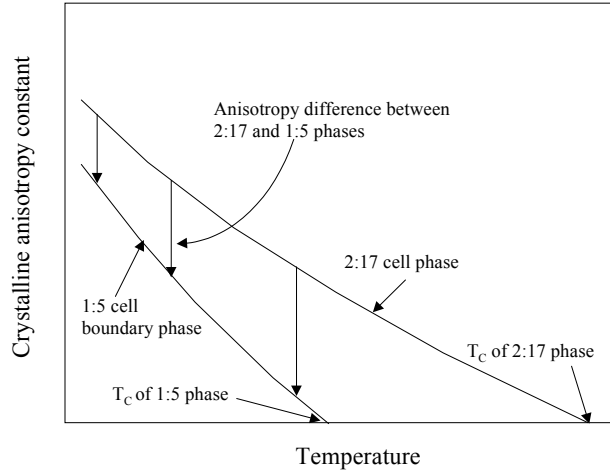


Figure 3-29: Schematic temperature dependence of crystalline anisotropy of 2:17 cell phase and 1:5 cell boundary phase.

Mechanism II – Thermal activation of domain walls

Since pinning is responsible for higher MH_c at higher temperature, the second coercivity mechanism that leads to lower MH_c at higher temperature has to be related to a process other than pinning. It is postulated that the second mechanism is closely related to a thermal activation process. This assumption is based on experimental data obtained in 1981 (Liu, S. et al. 1982) when it was observed that the temperature dependence of a 2:17 magnet could be exactly fitted to a simple exponential equation when the temperature was lower than 900K. It is believed that this was not an accident, but revealed the nature of the coercivity mechanism in 2:17 type magnets.

As mentioned previously, coercivity in 2:17-type magnets originates from domain wall pinning in the 1:5 cell boundary phase of the cellular microstructure. In order for the domain walls to break away from the 1:5 cell boundary phase, they must obtain enough energy to overcome the energy barrier between the 1:5 and 2:17 phases, namely ΔE . This energy can be acquired not only from the applied magnetic field (magnetic energy), but also from the thermal energy. It is easy to understand that the higher the temperature, the higher the thermal energy will be; and the domain walls that are in a thermal excited condition would have more chance to climb up the energy barrier. Assuming that the probability ρ of a domain wall to climb up an energy barrier ΔE at temperature T follows the Arrhenius equation,

$$\rho = C \exp(-\Delta E / k_B T), \quad (2)$$

where C is a constant and k_B is the Boltzmann constant. Apparently, high ρ means low coercivity. Thus, the relationship between MH_c and temperature T can be expressed as:

$$MH_c = c \exp(\Delta E(T) / k_B T), \quad (3)$$

where, c is a constant, and the energy barrier is written as $\Delta E(T)$ to emphasize that it is a function of temperature. It is apparent that $\Delta E(T)$ is the domain wall energy difference between the 2:17 and 1:5 phases and it can be written as:

$$\Delta E(T) = E_{2:17} - E_{1:5} = C_1 \sqrt{A_{2:17} K_{2:17}} - C_2 \sqrt{A_{1:5} K_{1:5}}, \quad (4)$$

where $A_{2:17}$ and $A_{1:5}$ are exchange constants; $K_{2:17}$ and $K_{1:5}$ are crystalline anisotropy constants for the 2:17 and 1:5 phases, respectively; and C_1 and C_2 are constants. Because the exchange constant A of a ferromagnetic material is a function of its Curie temperature, T_C , it can be written as:

$$A = c k_B T_C, \quad (5)$$

where k_B is Boltzmann constant and c is a constant. Substituting Equation 4 into Equation 3 and redefining the constants gives

$$\Delta E(T) = c_1 \sqrt{k_B(T_C)_{2:17} K_{2:17}} - c_2 \sqrt{k_B(T_C)_{1:5} K_{1:5}}. \quad (6)$$

Substituting Equation 6 into Equation 3, and considering that K is a function of T , we have

$$M H_c = c \exp\left(\frac{c_1 \sqrt{k_B(T_C)_{2:17} K(T)_{2:17}} - c_2 \sqrt{k_B(T_C)_{1:5} K(T)_{1:5}}}{k_B T}\right). \quad (7)$$

In a phenomenological sense, many transition phenomena affected by temperature follow the Arrhenius equation. Examples include (i) transition of electrons from a metal to a lightly-doped semiconductor (a sub-atomic scale transition); (ii) diffusion of atoms (an atomic scale transition); (iii) transition of a dislocation in crystals (a transition of an object with two dimensions in atomic scale); and (iv) transition of grain boundary (a transition of an object with one dimension in atomic scale). The domain wall transition is, in a sense, like the transition of grain boundary. In both cases, the objects of the transition possess only one dimension in atomic scale. However, when a domain wall moves, atoms actually do not move. What moves is only a narrow region in which the direction of magnetic moment differs from its neighbors. This is an important difference between domain wall and other objects that follow the Arrhenius equation. In addition, under a constant applied magnetic field, the thermal energy would play a critical role in domain wall transition and the time-dependent effect occurs. This would be the nature of magnetic viscosity phenomenon.

Explanation of various temperature dependencies of coercivity using the new model

According to this model, by modifying the compositions of the 1:5 cell boundary phase and the 2:17 cell phase, various temperature dependencies of the exponential $\Delta E(T)/k_B T$ can be obtained. There are six different possibilities:

- (1) With increasing temperature, $\Delta E(T)$ decreases. In this case, $\Delta E/k_B T$ decreases rapidly with temperature, which results in a large negative temperature coefficient of $M H_c$, as observed in conventional 2:17 magnets (Figure 3-9, magnet 1);
- (2) With increasing temperature, $\Delta E(T)$ increases at a smaller rate than T. In this case, $\Delta E(T)/k_B T$ decreases slowly with temperature, which results in a small negative temperature coefficient of $M H_c$, as observed in some newly-developed high temperature magnets (Figure 3-9, magnets 2, 3);
- (3) With increasing temperature, $\Delta E(T)$ increases at the same rate as T. In this case, $\Delta E(T)/k_B T$ is virtually a constant and independent of T, which results in a temperature-independent $M H_c$, as observed in some newly-developed high temperature magnets (Figure 3-9, magnet 4);
- (4) With increasing temperature, $\Delta E(T)$ remains the same and is independent of T, which results in a typical exponential relationship between $M H_c$ and T;
- (5) With increasing temperature, $\Delta E(T)$ increases at a larger rate than T. In this case, $\Delta E(T)/k_B T$ increases with temperature, which results in a positive temperature coefficient of $M H_c$;
- (6) $\Delta E(T)$ changes differently with temperature at different temperature ranges, which results in a complex temperature dependence of coercivity as observed in some newly-developed high temperature magnets (Figure 3-9, magnet 6).

As mentioned previously, coercivity mechanisms in permanent magnets are very complicated and many factors affect the coercivity development. It is believed that Equation 7 reveals the primary nature of coercivity mechanisms in 2:17-type permanent magnets. Other factors that influence the coercivity, such as the geometry of the cellular structure and the width of the 1:5 cell boundary phase, could be attributed to a modification of the constant c or the addition of other terms in Equation 7.

Calculations of Temperature Dependence of $M H_c$ Using the Proposed Model

The temperature dependence of $M H_c$ was calculated using Equation 7. In the calculations, three $\Delta E(T)$ cases were assumed. In each case, the calculated result is in good agreement of the observed experimental result.

Case I. $\Delta E(T)$ decreases with T. The assumed temperature dependence of crystalline anisotropy constants of the 2:17 cell phase and the 1:5 cell boundary phase is shown in Figure 3-30. The calculated result is shown in Figure 3-31. This case results in a large negative temperature coefficient, as observed in conventional 2:17 magnets (Figure 3-9, magnet 1);

Case II. $\Delta E(T)$ increases with T. The assumed temperature dependence of crystalline anisotropy constants of the 2:17 cell phase and the 1:5 cell boundary phase is shown in Figure 3-32. The calculated result is shown in Figure 3-33. This case results in a small negative temperature coefficient, as observed in some newly developed high temperature 2:17 magnets (Figure 3-9, magnet 3);

Case III. $\Delta E(T)$ increases rapidly with T at high temperature range (500 to 800 K). The assumed temperature dependence of crystalline anisotropy constants of the 2:17 cell phase and the 1:5 cell boundary phase is shown in Figure 3-34, and the calculated result is shown in Figure 3-35. This case results in complex temperature dependence, as observed in some newly-developed high temperature 2:17 magnets.

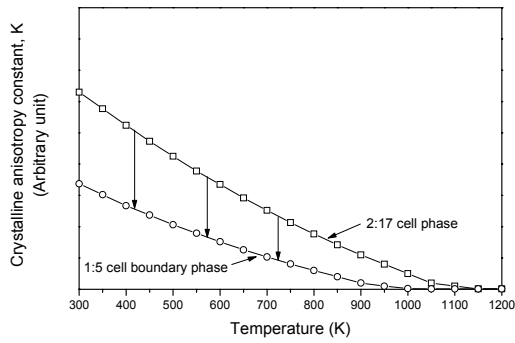


Figure 3-30. Assumed temperature dependence of crystalline anisotropy constant for 2:17 cell phase and 1:5 cell boundary phase. Case I, $\Delta E(T)$ decreases with T.

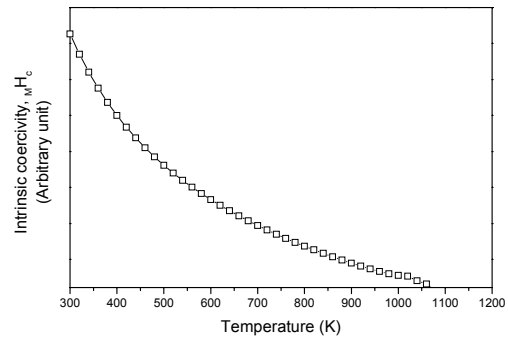


Figure 3-31. Calculated temperature dependence of M_{H_c} . Case I, $\Delta E(T)$ decreases with T.

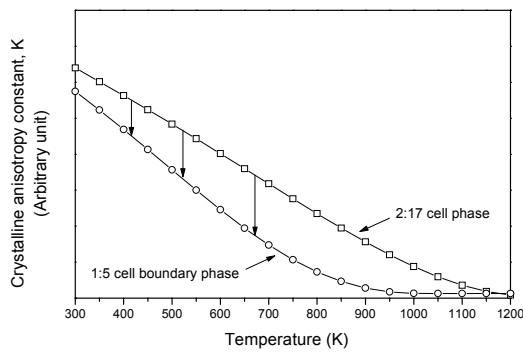


Figure 3-32. Assumed temperature dependence of crystalline anisotropy constant for 2:17 cell phase and 1:5 cell boundary phase. Case II, $\Delta E(T)$ increases with T.

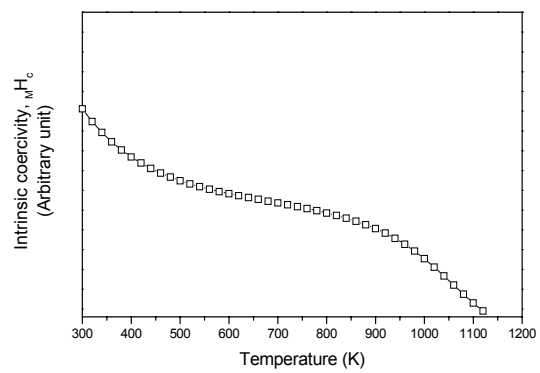


Figure 3-33. Calculated temperature dependence of M_{H_c} . Case II, $\Delta E(T)$ increases with T.

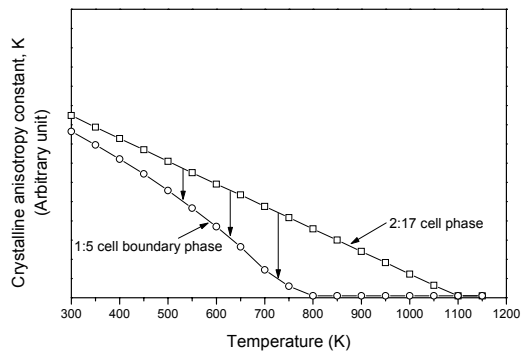


Figure 3-34. Assumed temperature dependence of crystalline anisotropy constant for 2:17 cell phase and 1:5 cell boundary phase. Case III, $\Delta E(T)$ increases rapidly with T.

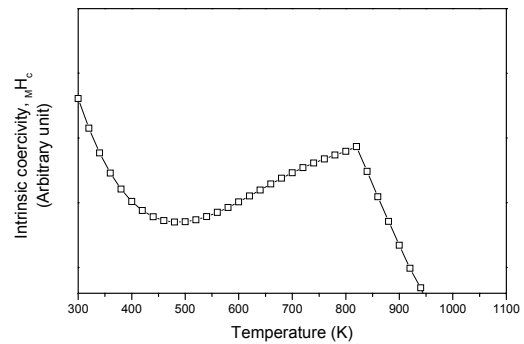


Figure 3-35. Calculated temperature dependence of M_{H_c} . Case III, $\Delta E(T)$ increases rapidly with T.

The new model of coercivity can satisfactorily explain not only the abnormal temperature dependence of MH_c shown in Figures 3-27 and 3-28, but also the “normal” temperature dependence of MH_c in conventional 2:17 magnets. This is because the two conflicting mechanisms exist not only in magnets with abnormal temperature dependence of MH_c , but in all 2:17 type permanent magnets. For conventional 2:17 magnets, the pinning mechanism is relatively weak at high temperatures and the thermal activation mechanism dominates at the entire temperature range. However, in the newly-developed magnets, the pinning mechanism is so strong at high temperatures that the magnets demonstrate small negative or even positive temperature coefficients of MH_c .

It is believed that this thermal activation-pinning model also applies to magnets that are controlled by crystalline anisotropy and domain wall pinning. This concept may apply to all ferromagnetic materials in which domain wall motion is involved during magnetization and demagnetization. For example, in soft magnetic materials the coercivity is determined by the maximum resistance to the domain wall motion. This resistance can be caused by any crystal imperfection, including grain boundaries, inclusions, precipitates, strain, and stress. The energy necessary for the domain walls to overcome an energy barrier $\Delta E(T)$ can be obtained not only from magnetic energy, but also from thermal energy $k_B T$. In general, the susceptibility of a soft magnetic material may be expressed as

$$\kappa \propto \exp(k_B T / \Delta E(T)). \quad (8)$$

However, since the domain walls in soft magnetic materials are quite thick resulting from the low magneto-crystalline anisotropy, thermal activation of domain walls in soft magnetic materials is probably more difficult than in magnetic materials with high crystalline anisotropy.

4. New approach to calculating temperature coefficients of magnetic properties

Permanent magnets with improved high temperature performance are needed for advanced systems. This requires not only developing new high temperature permanent magnets, but also a better and more accurate description of the temperature characteristics of magnetic materials. The most commonly-used parameter for temperature dependence of magnetic properties is the temperature coefficient. The temperature coefficient of a magnetic parameter Q over a temperature interval between T_1 and T_2 is defined as:

$$\alpha_{(T_1 \rightarrow T_2)} = \frac{Q_{T_2} - Q_{T_1}}{Q_{T_1}(T_2 - T_1)} \times 100 \text{ } (\% / ^\circ C). \quad (9)$$

The temperature coefficient of Q at a specific temperature T is defined as

$$\alpha_{T(\Delta T=0)} = \frac{\Delta Q}{Q \Delta T} \times 100 \text{ } (\% / ^\circ C). \quad (10)$$

It is obvious that $\alpha_{(T_1 \rightarrow T_2)}$ is an average of temperature coefficients of Q over the temperature interval $T_1 \rightarrow T_2$. However, $\alpha_{(T_1 \rightarrow T_2)}$ is not necessarily an accurate

description of the temperature dependence of Q , especially when the interval between T_1 and T_2 is large. Further, when Q is not a monotonous function of temperature T , Equation (9) may give a misleading result. On the other hand, α_T gives the temperature coefficient of Q at a specific temperature T . It is the “true” (or instantaneous) temperature coefficient and is a more accurate description of the temperature dependence of Q . Unfortunately, in practice, it is impossible to calculate α_T when $\Delta T = 0$ by simply using Equation (10).

The above-mentioned problem can be readily resolved if a polynomial is used to represent Q ,

$$Q(T) = a_0 + a_1T + a_2T^2 + \dots + a_nT^n = \sum_{i=0}^n a_iT^i, \quad (11)$$

and redefine the temperature coefficient of Q at T as:

$$\alpha_T = \frac{dQ}{dT} \times \frac{1}{Q} \times 100 \text{ (\%/}^\circ\text{C)}. \quad (12)$$

Coefficients $a_0, a_1, a_2, \dots, a_n$ in Equation (11) can be determined using a least squares fit. Calculating the derivative of this polynomial with respect to T yields

$$\frac{dQ}{dT} = a_1 + 2a_2T + 3a_3T^2 + \dots + na_nT^{n-1} = \sum_{i=1}^n ia_iT^{i-1}. \quad (13)$$

Substituting (11) and (13) into (12) leads to

$$\alpha_T = \frac{\sum_{i=1}^n ia_iT^{i-1}}{\sum_{i=0}^n a_iT^i} \times 100 \text{ (\%/}^\circ\text{C)} \quad (14)$$

Using Equation (14), the “true” temperature coefficients α_T of any magnetic parameter Q at any temperature T can be readily determined and a plot of temperature coefficient versus temperature (α_T vs. T) can be drawn. Normally, since α_T is more sensitive to T than Q , the α_T vs. T plot is a very useful tool to represent the temperature characteristics of a magnetic parameter. The average temperature coefficient $\alpha_{(T1 \rightarrow T2)}$ can be also calculated using Equation (11). The calculated results are very close to those determined by conventional method.

As an example, Figure 4-1 shows the temperature dependence of magnetization at 10 kOe of a commercial sintered $\text{Gd}_2(\text{Co,Fe,Cu,Zr})_{17}$ magnet. In the figure, the squares represent the experimental data, while the curve is a 6th degree polynomial fit. In any experimental characterization, random errors are always associated with the results of measurements. The least square fit eliminates those random errors and therefore the numerical result is generally a better representation in comparison to the original experimental data.

Figures 4-2 through 4-4 are plots of temperature coefficients of magnetization, intrinsic coercivity and maximum energy product versus temperature for some sintered rare earth permanent magnets. This concept can be further developed for modeling of temperature coefficients of magnetization for temperature compensated rare earth permanent magnets. See Section 6 for further details .

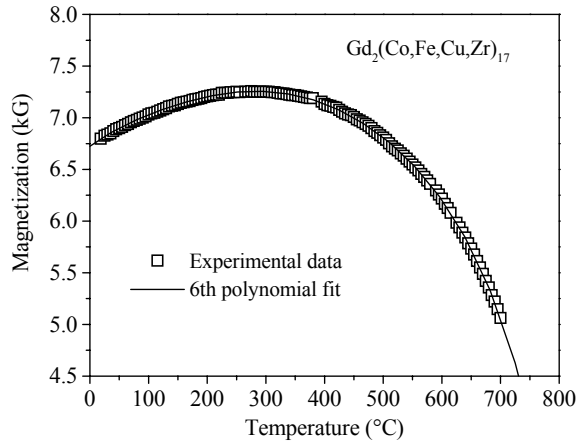


Figure 4-1. Temperature dependence of magnetization at 10 kOe of $Gd_2(Co,Fe,Cu,Zr)_{17}$.

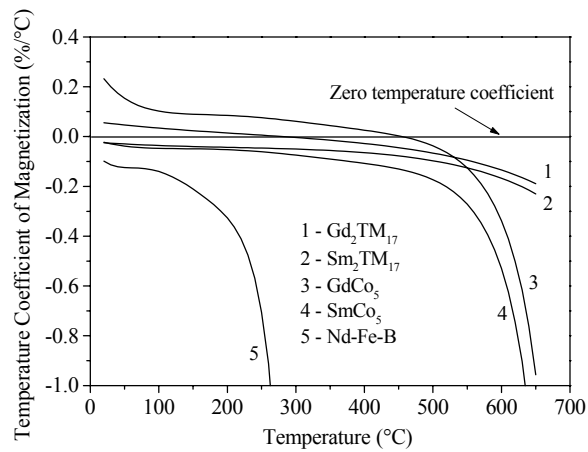


Figure 4-2. Temperature coefficients of magnetization at 10 kOe of some rare earth permanent magnets.

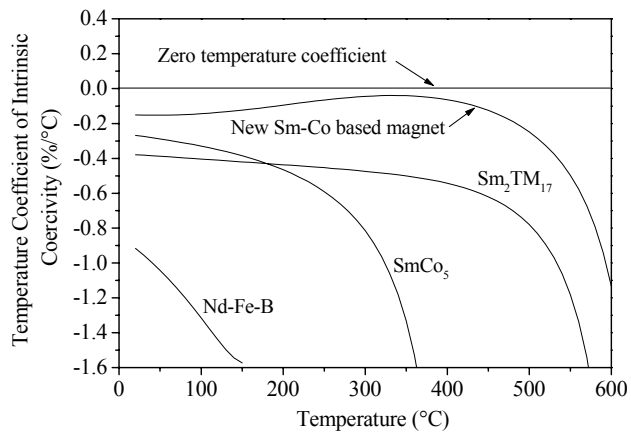


Figure 4-3. Temperature coefficient of intrinsic coercivity of some rare earth permanent magnets.

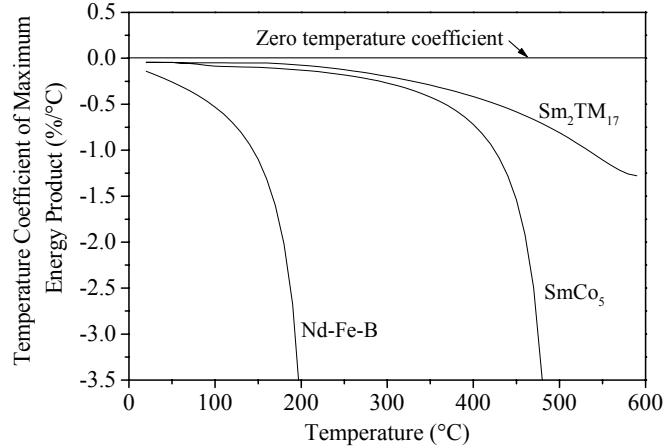


Figure 4-4. Temperature coefficient of maximum energy product of some rare earth permanent magnets.

5. SmCo₇-type permanent magnets

The Sm₂Co₁₇ compound has moderate high saturation magnetization and magneto-crystalline anisotropy and the highest Curie temperature (920°C) among all rare earth-transition metal compounds. However, it has proved very difficult to develop high coercivity in a pure Sm₂Co₁₇ compound. To develop useful coercivity, a considerable amount of non-magnetic elements, such as Cu and Zr, must be added, which results in significantly reduced magnetization and energy product. Another disadvantage of the current Sm₂(Co,Fe,Cu,Zr)₁₇ magnets is that a long-term heat treatment is necessary to develop high coercivity.

SmCo₇ phase is a metastable binary phase in the Sm-Co binary system, and it has a TbCu₇ crystal structure which can be derived from SmCo₅ (Wallace et al. 1980, Saito et al. 1989). The SmCo₇ compound has saturation magnetization and a Curie temperature lower than Sm₂Co₁₇ but higher than SmCo₅ compound. It has been reported that the metastable SmCo₇ phase can be obtained by melt spinning (Saito et al. 1989), splat cooling (Buschow et al. 1973), or mechanical alloying (Yang et al. 1996). It has also been reported that some transition metals such as Zr and Ti can stabilize SmCo₇ phase (Huang et al. 1998). Recently, P. Liu reported that high coercivity and positive temperature coefficient of coercivity were obtained without aging in SmCo_{7-x}Ti_x and SmCo_{7-x-y}Cu_xTi_y cast alloys. If the Ti and/or Ti, Cu substitutions can be made very low, and if the Fe substitution for Co can effectively enhance the saturation magnetization as it does in the Sm₂(Co,Fe)₁₇ system, then it would be possible for these 1:7-based compounds to have a virtually higher saturation magnetization than Sm₂(Co,Fe,Cu,Zr)₁₇ magnets. In addition, if high coercivity can be developed without long-term aging, it would also be a very significant factor in cutting the cost of production. Therefore, efforts have been made to explore the possibility of synthesizing sintered anisotropic magnet materials based on SmCo₇ phase (Liu, S. et al. 2000d).

It was found that a small amount of Ti addition stabilizes the 1:7 structure in Sm(Co_{1-v-x-y}Fe_vCu_xTi_y)_z with v = 0 - 0.15, x = 0 - 0.14, y = 0 - 0.08, and nominal z =

6.1 - 7.0. Fe substitution for Co increases remanence, but decreases coercivity. Cu increases coercivity, but decreases remanence. A peak coercivity was obtained with $x = 0.105$ in $\text{Sm}(\text{Co}_{\text{bal}}\text{Cu}_x\text{Ti}_{0.043})_{6.4}$ (6.4 is a nominal z value. Its corresponding effective z value is 7.0). The intrinsic coercivity was found to be sensitive to Ti content. A peak coercivity of over 4 kOe was obtained when $y = 0.04$ in $\text{Sm}(\text{Co}_{\text{bal}}\text{Cu}_{0.085}\text{Ti}_y)_{6.4}$. On the other hand, the magnetic properties were not very sensitive to the z value in $\text{Sm}(\text{Co}_{0.872}\text{Cu}_{0.085}\text{Ti}_{0.043})_z$ when nominal $z = 6.1-7.0$. The best room temperature intrinsic coercivity obtained in a Cu-free magnet of $\text{Sm}(\text{Co}_{0.957}\text{Ti}_{0.043})_{6.4}$ was 1.8 kOe. It was 4.5 kOe in a Cu-containing magnet of $\text{Sm}(\text{Co}_{0.875}\text{Cu}_{0.085}\text{Ti}_{0.04})_{6.4}$ and 7.1 kOe in a Hf modified $\text{Sm}(\text{Co}_{0.80}\text{Cu}_{0.16}\text{Hf}_{0.04})_6$. The best room temperature maximum energy product $(\text{BH})_{\text{max}}$ was 17.7 MGOe in a sintered anisotropic $\text{Sm}(\text{Co}_{0.80}\text{Cu}_{0.16}\text{Hf}_{0.04})_6$ magnet. These properties were achieved after rapidly quenching from the sintering temperature without aging. The coercivity mechanism remains unknown. It is anticipated that further adjustments of composition and heat treatment will lead to improved magnetic properties in sintered magnets based on SmCo_7 phase.

As mentioned in Section 3, the nominal z values of the newly developed high-temperature magnets are also close to 7. The difference between the aged SmTM_{-7} and the quenched SmCo_{-7} -based magnets described in this section is not only the fact that the latter may contain more Sm. The fundamental difference is that the coercivity in the SmTM_7 magnets is developed in a long-period aging. These magnets have a fine-scaled cellular microstructure consisting of three phases: a 2:17 cell phase with a rhombohedral structure, a 1:5 cell boundary phase with a hexagonal structure, and a Zr-rich platelet phase with a hexagonal structure. While the SmCo_{-7} -based magnets are supposed to be single-phased alloys with a 1:7 hexagonal structure without any fine-scaled microstructure.

6. Temperature compensated rare earth permanent magnets and modeling of temperature coefficient of magnetization

Permanent magnets with very low temperature coefficients of magnetic properties over a wide temperature range are required for many applications. Examples are microwave tubes, gyros, accelerometers, and conventional moving-coil meters. The flux provided by most permanent magnets decreases on heating. This is an intrinsic property for all ferromagnetic materials in which the saturation magnetization will eventually drop to zero at Curie temperature. To compensate this magnetization loss with increasing temperature, partial heavy rare earth substitution is used (Benz et al. 1974, Jones et al. 1976, Li et al. 1983, Liu, S. et al. 1990, Walmer et al. 1998). This temperature compensation is based on the fact that in rare earth-transition metal (RE-TM) compounds the magnetic moment coupling between RE and TM atoms depends on the type of RE used in the alloy. When RE is a light rare earth such as Ce, Pr, Nd, Sm, the moment couples parallel to the TM moment (ferromagnetic coupling). The compound moment in this case exhibits a decrease with increasing temperature over the entire temperature range up to the Curie temperature. By contrast, when the RE is a heavy rare earth such as Gd, Tb, Dy, Ho, Er, etc. the moment couples antiparallel to the TM-moment (ferrimagnetic coupling). For ferrimagnetic materials, variations of the HRE-TM compounds with temperature are complex and it is possible that in a certain temperature range the compound moment increases, rather than decreases, with increasing temperature.

Figure 6-1 shows magnetization versus temperature (upper) and temperature coefficient of magnetization versus temperature (lower), respectively. This figure defines some important terms used in temperature compensation as follows:

- T_p : Temperature corresponding to the peak magnetization.
 Temperature coefficient of magnetization (α) is zero at T_p .
- T_{min} to T_{max} : Temperature range for optimum temperature compensation. At T_{min} the temperature coefficient of magnetization is δ , at T_{max} it is $-\delta$. The magnitude of δ depends on applications. In most cases $d < 0.005\%/^{\circ}\text{C}$.

Good temperature compensated permanent magnets should have the following characteristics:

- High T_p . Or, for a particular application, a fixed T_p .
- Low T_{min} , high T_{max} . Or, large optimum compensation temperature range. In this range, $|\alpha| \leq \delta$.
- Small δ .

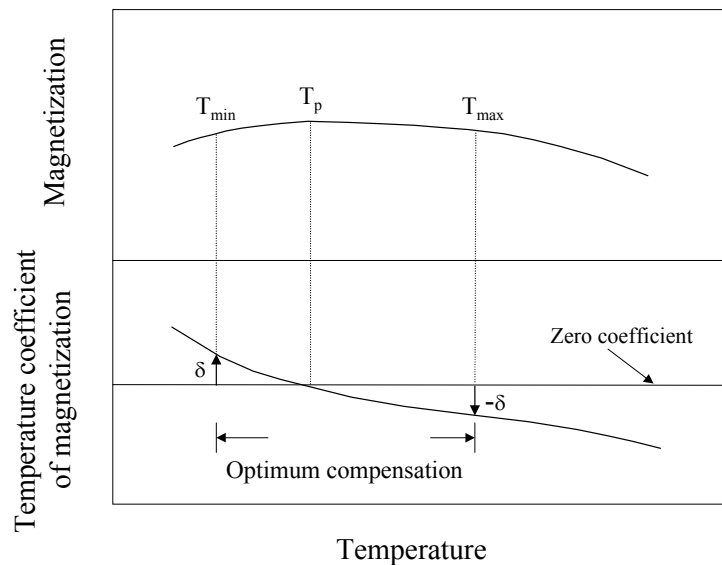


Figure 6-1. Temperature dependence of magnetization and temperature coefficient of magnetization.

Gd has been used for temperature compensation in both 1:5 and 2:17 types of rare earth permanent magnets. Temperature compensated magnets using partial Gd substitution for Sm illustrate very small temperature coefficients from -50°C to about 150°C with a peak magnetization at around room temperature. Higher T_p and a large temperature range for compensation are need for many applications. In addition to Gd, other heavy rare earths, such as Er and Ho can be also used for temperature compensation. Table 6-1 compares a few heavy rare earth 2:17-type compounds. It can be seen from the table that $\text{Er}_2\text{TM}_{17}$ has the highest magnetization, while $\text{Ho}_2\text{TM}_{17}$ has the highest T_p . Previous experiments indicated that $\text{Gd}_2\text{TM}_{17}$ has high

coercivity, but both $\text{Er}_2\text{TM}_{17}$ and $\text{Ho}_2\text{TM}_{17}$ showed low coercivity. Thus, it would be difficult to make a good temperature compensated magnet by using only a single heavy rare earth. To obtain a temperature compensated permanent magnet with a high coercivity, a high magnetization, a high temperature for the peak magnetization, and a large temperature range for compensation, it seems Gd, Er, Ho, and probably more heavy rare earths would have to be used. This typically requires considerable laboratory effort to determine the optimum combination of the light rare earth and the heavy rare earths. In research practice, a method of blending powders is often used. For example, by melting only two alloys of SmCo_5 and GdCo_5 , any magnet alloys that have the composition of $(\text{Sm}_{1-x}\text{Gd}_x)\text{Co}_5$, with $0 < x < 1$ can be obtained by blending powders of SmCo_5 and GdCo_5 .

Table 6-1. Comparison of a few heavy rare earth 2:17-type compounds.

| Compound | Peak magnetization (emu/g) | Temperature corresponding to peak magnetization, T_p ($^{\circ}\text{C}$) | Coercivity |
|-----------------------------|----------------------------|---|------------|
| $\text{Gd}_2\text{TM}_{17}$ | 60 | 300 | High |
| $\text{Er}_2\text{TM}_{17}$ | 70 | 250 | Low |
| $\text{Ho}_2\text{TM}_{17}$ | 63 | 400 | Low |

Because saturation magnetization ($4\pi M_s$) is an intrinsic property, it is possible to calculate the temperature coefficient of $4\pi M_s$ for a temperature compensated RE-TM magnet using a simple model that the magnetization of a $(\text{LRE}_{1-x}\text{HRE}_x)\text{-TM}$ compound is independently contributed by LRE-TM and HRE-TM. As a first step of the modeling, the temperature dependence of $4\pi M_s$ for SmCo_5 and GdCo_5 alloys should be experimentally determined by obtaining two functions $M_1(T)$ and $M_2(T)$. Then, two polynomials can be used to represent these functions. Following that, these two polynomials can be “blended” (added) instead of blending two alloys, obtaining a third polynomial,

$$M_3(T) = (1-x) M_1(T) + x M_2(T), \quad (15)$$

where $0 \leq x \leq 1$. Next, the derivative of $M_3(T)$ with respect to T , $dM_3(T)/dT$ can be easily determined. Finally, the temperature coefficient of the new “alloy” at any specific temperature can be derived using

$$\alpha_T = \frac{dM_3(T)}{dT} \times \frac{1}{M_3(T)} \times 100 (\%/^{\circ}\text{C}) \quad (16)$$

In other words, the α_T versus T relationship for the new “alloy” can be readily established.

The concept of calculating $4\pi M_s$ in HRE-substituted rare earth permanent magnets was first proposed by F. E. Camp and B.M. Ma, et al. (Camp et al. 1985, Ma et al. 1986). However, the approach they used for the calculation and the algorithms they employed were not mentioned. S. Liu (Liu et al. 1990a,b) then proposed using a polynomial to represent the temperature dependence of saturation magnetization and

moved one step forward by proposing to calculate the temperature coefficients of (LRE_{1-x}-HRE_x)-TM systems.

Using this approach, S. Liu et al. (Liu et al. 1999b) calculated the temperature coefficients of magnetization of the (Sm_{1-x}Gd_x)Co₅ and (Sm_{1-x}Gd_x)₂(Co,Fe,Cu,Zr)₁₇ systems with 0 ≤ x ≤ 1 in the temperature range of 20 to 600°C. In a plot of α_T vs. T, when α_T changes its sign from positive to negative, the α_T vs. T curve crosses the line of α_T = 0, and determines the temperature at which the temperature coefficient becomes zero for magnets with various HRE contents. The temperatures corresponding to the zero temperature coefficients of the magnetization at 10 kOe applied field for (Sm_{1-x}Gd_x)Co₅ and (Sm_{1-x}Gd_x)₂(Co,Fe,Cu,Zr)₁₇ systems with 0 ≤ x ≤ 1 were determined and the temperature compensation effect of Gd in these two systems was compared.

Figure 6-2 is a plot of the temperature coefficient of magnetization at 10 kOe of (Sm_{1-x}Gd_x)Co₅ versus temperature. The temperatures corresponding to zero temperature coefficients for magnets with various Gd contents are summarized in Table 6-2. The effects of Gd compensation on the temperature coefficients of magnetization in (Sm_{1-x}Gd_x)Co₅ and (Sm_{1-x}Gd_x)₂(Co,Fe,Cu,Zr)₁₇ systems are summarized in Figure 6-3. Figure 6-3 also shows the variation of magnetization of (Sm_{1-x}Gd_x)Co₅ and (Sm_{1-x}Gd_x)₂(Co,Fe,Cu,Zr)₁₇ versus Gd content. It is obvious from Table 6-2 and Figure 6-3 that Gd shows a much stronger effect for temperature compensation in the (Sm_{1-x}Gd_x)Co₅ system than in the (Sm_{1-x}Gd_x)₂(Co,Fe,Cu,Zr)₁₇ system. However, it must also be noted that the temperature compensation effects are at the expense of magnetization in both systems.

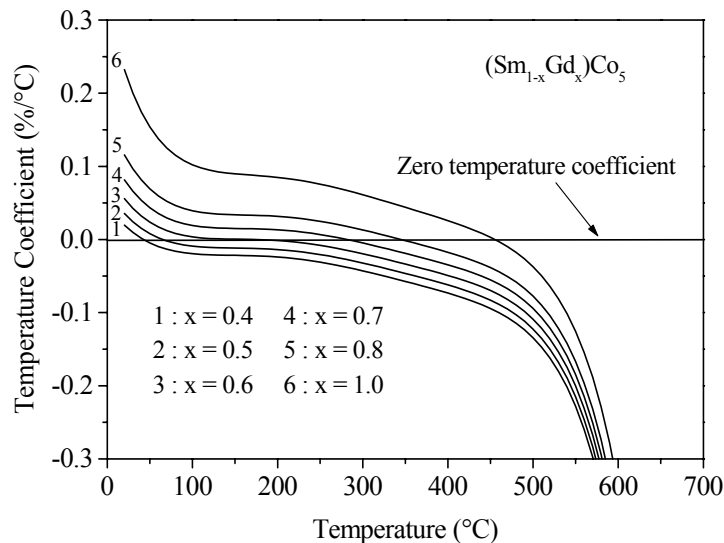


Figure 6-2. Temperature coefficient of magnetization at 10 kOe of (Sm_{1-x}Gd_x)Co₅ versus temperature.

Table 6-2. Temperatures for zero temperature coefficient of magnetization for $(\text{Sm}_{1-x}\text{Gd}_x)\text{Co}_5$ and $(\text{Sm}_{1-x}\text{Gd}_x)_2(\text{Co,Fe,Cu,Zr})_{17}$ magnets

| Gd content (x) | Temperature for zero temperature coefficient (°C) | |
|----------------|---|--|
| | $(\text{Sm}_{1-x}\text{Gd}_x)\text{Co}_5$ | $(\text{Sm}_{1-x}\text{Gd}_x)_2\text{TM}_{17}$ |
| 0.4 | 42 | 0 |
| 0.5 | 65 | 56 |
| 0.6 | 171 | 80 |
| 0.7 | 281 | 157 |
| 0.8 | 345 | 214 |
| 1.0 | 455 | 277 |

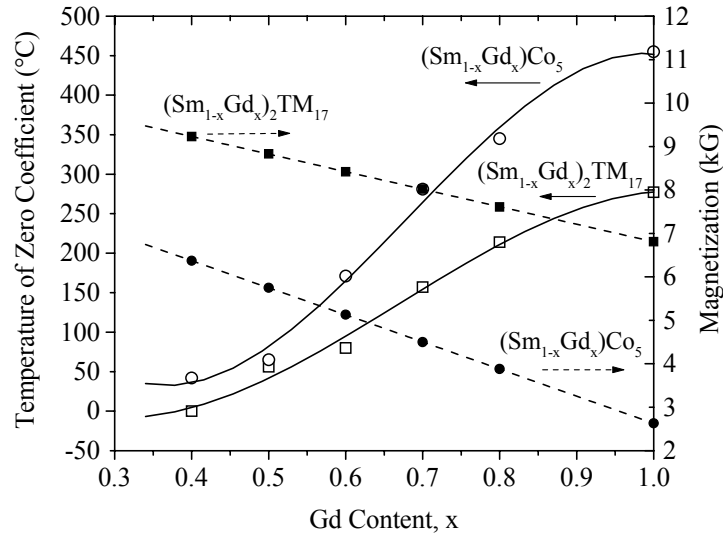


Figure 6-3. Temperature for zero temperature coefficient of magnetization and magnetization versus Gd content in $(\text{Sm}_{1-x}\text{Gd}_x)\text{Co}_5$ and $(\text{Sm}_{1-x}\text{Gd}_x)_2\text{TM}_{17}$ systems.

The numerical expression of this approach is simple. Let's start from a (LRE-HRE)-TM system. Suppose the temperature dependencies of magnetization for LRE-TM and HRE-TM are represented by m-degree polynomials:

$$M_{LRE-TM}(T) = a_0 + a_1T + a_2T^2 + \dots + a_mT^m = \sum_{i=0}^m a_iT^i = f_1(T), \quad (17)$$

$$M_{HRE-TM}(T) = b_0 + b_1T + b_2T^2 + \dots + b_mT^m = \sum_{i=0}^m b_iT^i = f_2(T). \quad (18)$$

Coefficients $a_0, a_1, a_2, \dots, a_m$ and $b_0, b_1, b_2, \dots, b_m$ can be determined using a least squares fit. Assuming that $(n+1)$ experimental data points are obtained for the LRE-TM magnet alloy and the temperature corresponding to the j -th point is T_j . Then, the magnetization corresponding to the j -th point is Y_j ($j=0$ to n). An m -degree least squares fit corresponds to solving the following system of $m+1$ linear equations:

$$\begin{aligned}
(n+1)a_0 + \sum_{j=0}^n T_j a_1 + \sum T_j^2 a_2 + \dots + \sum T_j^m a_m &= \sum Y_j \\
\sum_{j=0}^n T_j a_0 + \sum T_j^2 a_1 + \sum T_j^3 a_2 + \dots + \sum T_j^{m+1} a_m &= \sum Y_j T_j \\
\sum T_j^2 a_0 + \sum T_j^3 a_1 + \sum T_j^4 a_2 + \dots + \sum T_j^{m+2} a_m &= \sum Y_j T_j^2 \quad (19) \\
&\vdots \\
&\vdots \\
&\vdots \\
\sum T_j^m a_0 + \sum T_j^{m+1} a_1 + \sum T_j^{m+2} a_2 + \dots + \sum T_j^{2m} a_m &= \sum Y_j T_j^m
\end{aligned}$$

Since T_j and Y_j are obtained experimentally, $a_0, a_1, a_2, \dots, a_m$ can be readily determined. Coefficients $b_0, b_1, b_2, \dots, b_m$ for the HRE-TM magnet can be determined using the same procedure. Because, as mentioned before, it is assumed that LRE-TM and HRE-TM independently contributes to the magnetization of (LRE-HRE)-TM, the variation of magnetization versus temperature for $(\text{LRE}_{1-x}\text{HRE}_x)$ -TM would be

$$\begin{aligned}
M_{(\text{LRE}_{1-x}\text{HRE}_x)\text{-TM}} &= (1-x)f_1(T) + x f_2(T) \\
&= (1-x) \sum_{i=0}^m a_i T^i + x \sum_{i=0}^m b_i T^i \\
&= \sum_{i=0}^m [(1-x)a_i + x b_i] T^i = f_3(T) \quad (20)
\end{aligned}$$

where x is the atomic fraction of the HRE.

The temperature coefficient of magnetization for the temperature-compensated magnet is

$$\alpha_T = \frac{d[f_3(T)]}{dT} x \frac{1}{f_3(T)} x 100 \text{ (\%/}^\circ\text{C)}$$

It is very easy to obtain the derivative of a polynomial,

$$\frac{d[f_3(T)]}{dT} = \frac{d}{dT} \sum_{i=0}^m [(1-x)a_i + x b_i] T^i = \sum_{i=1}^m i [(1-x)a_i + x b_i] T^{i-1} . \quad (21)$$

Therefore,

$$\alpha_T = \frac{\sum_{i=1}^m i[(1-x)a_i + xb_i]T^{i-1}}{\sum_{i=0}^m [(1-x)a_i + xb_i]T^i} \times 100 \text{ (\%/}^\circ\text{C)} \quad (22)$$

Now, let us consider RE-TM magnet alloys containing more than one HRE. Suppose the target magnet alloy contains k ($k > 2$) rare earths, that is to consider

$$[(RE_1)x_1 (RE_2)x_2 \dots RE_k)x_k]-TM$$

where RE_1, RE_2, \dots, RE_k stand for different rare earths (either LRE or HRE) and x_1, x_2, \dots, x_k are their atomic fractions and $x_1 + x_2 + \dots + x_k = 1$. The variations of magnetization of RE_1 -TM, RE_2 -TM, \dots , RE_k -TM versus temperature, determined by experiment, are represented by polynomials:

$$\begin{aligned} M_{RE_1-TM} &= \phi_1(T) = \sum_{i=0}^m a_{1i}T^i \\ M_{RE_2-TM} &= \phi_2(T) = \sum_{i=0}^m a_{2i}T^i \\ &\vdots \\ &\vdots \\ &\vdots \\ M_{RE_k-TM} &= \phi_k(T) = \sum_{i=0}^m a_{ki}T^i \end{aligned}$$

Again, assuming the magnetization of $[(RE_1)x_1 (RE_2)x_2 \dots RE_k)x_k]-TM$ is independently contributed by RE_1 -TM, RE_2 -TM, \dots , and RE_k -TM within the temperature range of the experiment, then, the variation of magnetization versus temperature for the magnet alloy is

$$\begin{aligned} &M_{[(RE_1)x_1 (RE_2)x_2 \dots (RE_k)x_k]-TM} \\ &= x_1\phi_1(T) + x_2\phi_2(T) + \dots + x_k\phi_k(T) \\ &= \sum_{i=0}^m (x_1a_{1i} + x_2a_{2i} + \dots + x_ka_{ki})T^i \\ &= \sum_{i=0}^m \left(\sum_{j=1}^k x_j a_{ji} \right) T^i = F(T) \end{aligned} \quad (23)$$

The temperature coefficient of magnetization for the magnet alloy, α_T , is

$$\alpha_T = \frac{dF(T)}{dT} \times \frac{1}{F(T)} \times 100 \text{ (\%/}^\circ\text{C)}$$

Or

$$\alpha_T = \frac{\sum_{i=1}^m i \left(\sum_{j=1}^k x_j a_{ji} \right) T^{i-1}}{\sum_{i=0}^m \left(\sum_{j=1}^k x_j a_{ji} \right) T^i} \times 100 \text{ (\%/}^\circ\text{C)} \quad (24)$$

Very good agreement was obtained between the calculated data and the experimentally determined results in $(\text{Sm}_{1-x}\text{Gd}_x)_2(\text{Co,Fe,Cu,Zr})_{17}$ in the temperature range of $-50^\circ\text{C} - 300^\circ\text{C}$. The soundness of this modeling approach in more complicated systems is to be confirmed by experiments.

As mentioned before, temperature compensated magnets using partial Gd substitution for Sm illustrate very small temperature coefficients from -50°C to about 150°C with a peak magnetization at around room temperature. Recently, in a temperature compensated magnet containing Er and Ho a very high T_p of 262°C was obtained. This T_p is more than 200°C higher than that of the $(\text{Sm}_{0.5}\text{Gd}_{0.5})_2\text{TM}_{17}$ magnet.

7. Other high-temperature permanent magnet materials

In order to significantly improve the performance of permanent magnets, the saturation magnetization ($4\pi M_s$) must be substantially increased since the upper limit of the maximum energy product of a permanent magnet is determined by $(4\pi M_s)^2/4$. This would require an effort to find new compounds containing more transition metal. Figure 7-1 illustrates saturation magnetization versus the Co content in the binary Sm-Co system. The saturation magnetization of LaCo_{13} compound is also included in the figure. It is obvious from Figure 7-1 that the saturation magnetization of the Sm-Co compounds enhances linearly with increasing the Co content. As displayed in Figure 2-1, the Curie temperature of the Sm-Co compound also enhances linearly with increasing the Co content.

The LaCo_{13} compound is the only stable 1:13-type compound found in all binary rare earth-transition metal systems. Because it has high concentration of Co, the LaCo_{13} compound possesses a very high Curie temperature of 1045°C and a high saturation magnetization of 13 kG at room temperature. Unfortunately, its cubic crystal structure and, hence, low magneto-crystalline anisotropy prevented it from being developed into permanent magnets (Velge et al. 1968, Ido et al. 1990). In recent years, M.Q. Huang, et al (Huang et al. 1995, 1996) studied the possibility of forming 1:13-type compounds in $\text{RECo}_{13-x}\text{Si}_x$ (RE = La, Pr, Nd, Gd, and Dy). Investigation should be carried out to explore the possibility of forming a SmCo_{13} compound by adding a third element and/or by using a special process because SmCo_{13} may have the highest magneto-crystalline anisotropy (see Section 2). If successful, another breakthrough in high-temperature permanent magnets is possible as indicated in Table 7-1. An assumption was made when estimating the saturation magnetization of $\text{Sm}(\text{Co}_{0.8}\text{Fe}_{0.2})_7$ and $\text{Sm}(\text{Co}_{0.8}\text{Fe}_{0.2})_{13}$ compounds that the effect of Fe on enhancing saturation magnetization in the 1:7 and 1:13 compounds is the same as

that in the 2:17 compound. This was partially confirmed in the 1:7 system as mentioned in Section 5.

It will be not easy to develop the next generation of high-temperature permanent magnets based on the SmCo_{13} compounds. If SmCo_{13} could be successfully made, its magneto-crystalline anisotropy would be low, probably much lower than those of $\text{Sm}_2\text{Co}_{17}$ and SmCo_5 compounds. It would then be a challenge to increase the coercivity by, for example, substitution without significantly decreasing the saturation magnetization and Curie temperature.

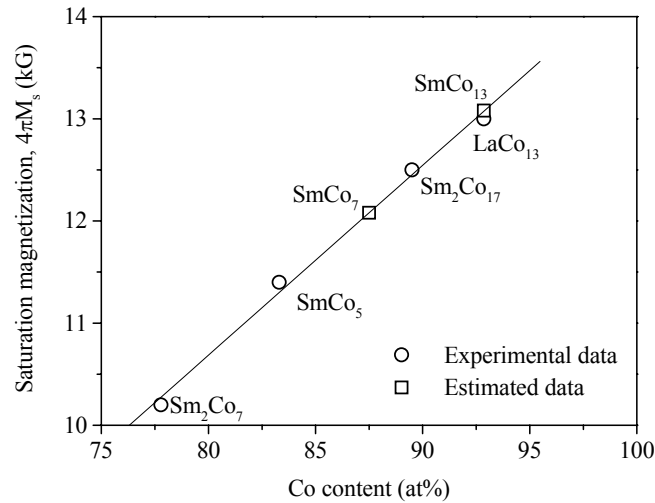


Figure 7-1. Saturation magnetization, $4\pi M_s$, of Sm-Co binary compounds versus Co content. $4\pi M_s$ of LaCo_{13} is also given in the figure.

Table 7-1. Saturation magnetization and Curie temperature of a few Sm-Co compounds.

| Compound | $4\pi M_s$ (kG) | Curie Point T_C ($^{\circ}\text{C}$) | Theoretical $(BH)_{\max}$ | Reference |
|---|-----------------|--|---------------------------|---------------|
| SmCo_5 | 11.4 | 727 | 32 | (Strnat 1988) |
| SmCo_7^* | 12.1 | 843 | 37 | estimated |
| $\text{Sm}(\text{Co}_{0.8}\text{Fe}_{0.2})_7^*$ | 13.7 | 801 | 47 | estimated |
| $\text{Sm}_2\text{Co}_{17}$ | 12.5 | 920 | 39 | (Strnat 1988) |
| $\text{Sm}_2(\text{Co}_{0.8}\text{Fe}_{0.2})_{17}$ | 14.0 | 870 | 49 | *** |
| $\text{Sm}_2(\text{Co}_{0.72}\text{Fe}_{0.2}\text{Cu}_{0.06}\text{Zr}_{0.02})_{7.4}^{**}$ | 12.0 | 820 | 36 | *** |
| SmCo_{13}^* | 13.3 | 1050 | 44 | estimated |
| $\text{Sm}(\text{Co}_{0.8}\text{Fe}_{0.2})_{13}^*$ | 15.0 | 1000 | 56 | estimated |

* Metastable compound

** Sintered magnet

*** University of Dayton magnetics Lab unpublished data

Acknowledgments

Most recent advances in high-temperature permanent magnets related to the author and his co-workers covered in this chapter were accomplished under the US Air Force and DARPA/ONR sponsorship. Special gratitude goes to Dr. Christina Chen of Electron Energy Corporation. Without her help and cooperation it would be impossible to finish this chapter. The author would like to thank Dr. G.E. Kuhl of University of Dayton, Mr. W. Gong, and Mr. M. Walmer of Electron Energy Corporation for their cooperation in the research programs. The author's gratitude also goes to Ms. N. Maxwell of the University of Dayton for editing the manuscript and to many of his colleagues who reviewed the manuscript and gave valuable comments and suggestions.

References

- Benz, M.G., Laforce, R.P., and Martin, D.L., AIP Conf. Proc. No. **18/2**, Eds C.D. Graham and J.J. Rhyne, 1173(1974)
- Buschow, K.H., and Broeder, F.J.A den, J. Less-Common Met, **3**, 191(1973)
- Camp, F. E., Narasimhan, K .S. V. L., and Hurt, J. C., IEEE Trans. Magn., **21**, 1970(1985)
- Chen, C.H., Walmer, M.S., Walmer, M.H., Liu, S., and Kuhl, E., J. Appl. Phys. **83**, 6706(1998)
- Fingers, R.T., and Rubertus, C.S., IEEE Trans. Magn. **36**, 3373(2000)
- Huang, M.Q., Wallace, W.E., Obermyer, R.T., Simizu, S., and Sankar, S.G., J. Magn. Mater. **151**, 150(1995)
- Huang, M.Q., Wallace, W.E., Obermyer, R.T., Simizu, S., McHenry, M., and Sankar, S.G., J. Appl. Phys. **79**, 5949(1996)
- Huang, M.Q., Wallace, W.E., and McHenry, M., J. Appl. Phys., **83**, 6718(1998)
- Ido, H., Sohn, J.C., Pourarian, F., Cheng, S.F., and Wallace, W.E., J. Appl. Phys. **67** 4978(1990)
- Jones, F.G. and Tokunaga, M., IEEE Trans Magn. **12**, 968(1976)
- Khan, Y., Proc. 11th Rare Earth Res. Conf. **II**, 652(1974)
- Kim, A.S., J. Appl. Phys. **83**, 6715(1998)
- Lecard, E., Allibert, C.H., and Ballou, R., J. Appl. Phys. **75**, 6277(1994)
- Li, D., Liu, J., Zhou, S., Jin, X., and Xu, E., Proc. 7th Int'l Workshop on REPM, 495(1983)
- Liu, J.F., Chui, T., Dimitrov, D., and Hadjipanayis, G. C., Appl. Phys. Let. **73**, 3007(1998)
- Liu, J. F., Zhang, Y., Dimitrov, D. and Hadjipanayis, G. C., J. Appl. Phys. **85**, 2800(1999a)
- Liu, J.F., Ding, Y., and Hadjipanayis, G. C., J. Appl. Phys. **85**, 1670(1999b)
- Liu, S., Mildrum H.F., and Strnat, K.J., J. Appl. Phys. **53**, 2383(1982)
- Liu, S., Ray, A.E., and Mildrum, H.F., J. Appl. Phys. **67**, 4975(1990)
- Liu, S., Ray, A.E. and Mildrum, H.F., Proc. 11th Int'l Workshop on REPM, 389(1990)
- Liu, S., and Hoffman, G.P., IEEE Trans. Magn. **32**, 5091(1996)
- Liu, S., Hoffman, G.P., and Brown J.R., IEEE Trans Magn. **33**, 3859(1997)
- Liu, S., Yang, J., Doyle, G., Kuhl, G.E., Chen, C., Walmer, M.S., and Walmer, M.H., IEEE Trans. Magn. **35**, 3325(1999a)

Liu, S., Kuhl, G.E., IEEE Magn. **35**, 3271(1999b)

Liu, S., Potts, G, Doyle, G., Yang, J., Kuhl, G.E., Chen, C, Walmer, M.S., and Walmer, M.H., IEEE Trans. Magn. **36**, 3297(2000a)

Liu, S., Yang, J., Doyle, G., Potts, G., Kuhl, G.E., Chen, C.H., Walmer, M.S., Walmer, M.H., J. Appl. Phys. **87**, 6728(2000b)

Liu, S., Kuhl, E., Chen, C., Walmer, M., Walmer, M., Gong, W., Proc. 16th Int'l Workshop of REPM, 159(2000c)

Liu, S., Kuhl, E., Chen, C., Walmer, M., Gong, W., Proc. 16th Int'l Workshop of REPM, 71(2000d)

Liu, S., Doyle, G., Kuhl, G.E., Chen, C., Walmer, M., Liu, Y., to be published in 2001 Livingston, J.D., and Martin, D.L., J. Appl. Phys. **48**, 2608(1977)

Ma, B-M., Narasimhan, K. S. V. L., and Hurt, J. C., IEEE Trans. Magn., **22**, 1081(1986)

Ma, B.M., Liang, Y.L., Patel, J., Scott, D., and Bounds, C.O., IEEE Trans. Magn. **32**, 4377(1996)

Mildrum, H.F., Krupar, J.B. , and Ray, A.E., J. Less-Commen Met. **93**, 261(1983)

Mishra, R.K., Thomas, G., Yoneyama, T., Fukuno, A., and Ojima, T., J. Appl. Phys. **52**, 2517(1981)

Perkins, R.S., Gaiffi, S. and Menth, A., IEEE Trans. Magn. **11**, 1431(1975)

Popov, A.G., Korolev, A.V., and Shchegoleva, N.N., Phys. Met. Metall. **69**, 100(1990)

Popov, A.G., Gaviko, V.S., Magat, L.M., and Ivanova, G.V., Phys. Met Metall. **70**, 18(1990)

Ray, A.E., and Strnat, K.J., IEEE Trans. Magn. **8**, 516(1972)

Ray, A.E., J. Appl. Phys. **55**, 2094(1984)

Ray, A.E., Soffa, W.A., Blachere, J.R., and Zhang, B., IEEE Trans. Magn. **23**, 2711(1987)

Ray, A.E., J. Appl. Phys. **67**, 4972(1990)

Ray, A.E. and Liu, S., L. Matl. Eng. and Perf., **1**, 183(1992)

Saito, H., Takahashi, M., Wakiyama, T., Kodo, G., and Nakagawa, H., J. Magn. Magn. **82**, 322(1989)

Schrefl, T., Fidler, J., and Scholz, W., IEEE Trans. Magn. **36**, 3394(2000)

Strnat, K.J., *Rare Earth-Cobalt Permanent Magnets*, Edited Wohlfarth, E.P. and Buchow, K.H.J., Elsevier Science Publishers B.V., 154(1988)

Velge, W.A.J.J., and Buschow, K.H.J., J Appl. Phys. **39** 1717 (1968)

Wallace, W.E. and Narasimhan, K.S., *Science and Technology of Rare Earth Materials*, 395(1980)

Walmer, M.S., Chen, C.H., Walmer, M.H., Liu, S., Kuhl, G.E., Proc. 15th Int'l Workshop on REPM, 689(1998)

Walmer, M.S., Chen, C.H., Walmer, M.H., Liu, S., and Kuhl, G.E., Proc. 16th Int'l Workshop of REPM, 41(2000a)

Walmer, M.S., Chen, C.H., and Walmer, M.H., IEEE Trans. Magn. **36**, 3376(2000b)

Yang, J., Mao, O., and Altounian, Z., IEEE Trans. Magn. **32**, 4390(1996)